

ADA 037009

(12) *J*  
RADC-TR-76-260  
Interim Technical Report  
August 1976



### IR WINDOW STUDIES

John H. Marburger

Electronic Sciences Laboratory  
University of Southern California  
Los Angeles, California 90007



Approved for public release; distribution unlimited

Sponsored by:

Defense Advanced Research Projects Agency (DoD)  
ARPA Order No. 2055

Monitored by: Deputy for Electronic Technology (RADC/ETSS)  
Hanscom AFB, MA 01731

Under Contract No. F19628-76-C-0162

ROME AIR DEVELOPMENT CENTER  
AIR FORCE SYSTEMS COMMAND  
GRIFFISS AIR FORCE BASE, NEW YORK 13441

COPY AVAILABLE TO DDC DOES NOT  
PERMIT FULLY LEGIBLE PRODUCTION

ARPA Order No. 2055

Program Code No. 3D10

Effective Date of Contract:  
1 September 1975

Contractor: University of  
Southern California

Contract No. F19628-76-C-0162

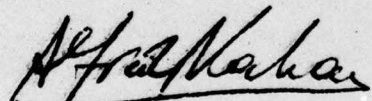
Principal Investigator and Phone No.:  
Prof. John H. Marburger, (213) 746-6213

RADC/ETSS Project Scientist and Phone No:  
Alfred Kahan, (617) 861-4014

Contract Expiration Date: 30 September 1976

*This report has been reviewed by the RADC Information Office (OI)  
and is releasable to the National Technical Information Service (NTIS).  
At NTIS it will be releasable to the General public, including foreign  
nations.*

*This technical report has been reviewed and is approved.*



ALFRED KAHAN  
Contract Monitor

ACCESSION for	
NTIS	White Section <input checked="" type="checkbox"/>
DOC	Buff Section <input type="checkbox"/>
UNANNOUNCED	<input type="checkbox"/>
JUSTIFICATION	
BY	
DISTRIBUTION/AVAILABILITY CODES	
DISL	AVAIL. AND OR SPECIAL
	

Qualified requestors may obtain additional copies  
from the Defense Documentation Center. All others  
should apply to the National Technical Information  
Service.

The views and conclusions contained in this  
document are those of the authors and should  
not be interpreted as necessarily representing  
the official policies, either expressed or  
implied, of the Defense Advanced Research  
Projects Agency or the U. S. Government.

UNCLASSIFIED

SECURITY CLASSIFICATION OF THIS PAGE (When Data Entered)

19 REPORT DOCUMENTATION PAGE			READ INSTRUCTIONS BEFORE COMPLETING FORM	
1. REPORT NUMBER RADC-TR-76-260		2. GOVT ACCESSION NO. ⑨ Interim rept. no. 1		3. RECIPIENT'S CATALOG NUMBER
4. TITLE (and Subtitle) IR WINDOW STUDIES		5. TYPE OF REPORT & PERIOD COVERED 1 Sep 75 - 31 Mar 76 Scientific - Interim No. 1		6. PERFORMING ORG. REPORT NUMBER
7. AUTHOR(s) John H. Marburger		8. CONTRACT OR GRANT NUMBER(s) F19628-76-C-0162 ARPA Order - 2055		10. PROGRAM ELEMENT, PROJECT, TASK AREA & WORK UNIT NUMBERS
9. PERFORMING ORGANIZATION NAME AND ADDRESS University of Southern California Electronic Sciences Laboratory Los Angeles, California 90007		11. CONTROLLING OFFICE NAME AND ADDRESS Defense Advanced Research Projects Agency 1400 Wilson Blvd. Arlington, VA 22209		12. REPORT DATE Aug 76
14. MONITORING AGENCY NAME & ADDRESS (if different from Controlling Office) Deputy for Electronic Technology (RADC/ETSS) Hanscom AFB, MA 01731 Monitor/Alfred Kahan		15. SECURITY CLASS. (of this report) UNCLASSIFIED		15a. DECLASSIFICATION/DOWNGRADING SCHEDULE 12 103p.
16. DISTRIBUTION STATEMENT (of this Report) Approved for public release; distribution unlimited				
17. DISTRIBUTION STATEMENT (of the abstract entered in Block 20, if different from Report)				
18. SUPPLEMENTARY NOTES This research was sponsored by Defense Advanced Research Projects Agency ARPA Order No. 2055				
19. KEY WORDS (Continue on reverse side if necessary and identify by block number) IR Windows II-VI Semiconductors Laser Damage Thermal Lensing Alkali Halides IR Absorption				
20. ABSTRACT (Continue on reverse side if necessary and identify by block number) This report describes progress on the first six months of effort on a program of infrared window studies. Studies related to thermal lensing include quantitative measurements of thermal lensing in CdTe, measurement of the three independent strain optic coefficients in CdTe and GaAs using an acousto-optic technique, and a theory of thermally induced birefringence in polycrystalline materials. Effort also focussed on defects in IR window materials, including a study of microscopic imperfections in CdTe and ZnSe in which the techniques (cont'd.)				

DD FORM 1473 EDITION OF 1 NOV 65 IS OBSOLETE  
JAN 73

UNCLASSIFIED

SECURITY CLASSIFICATION OF THIS PAGE (When Data Entered)

361620

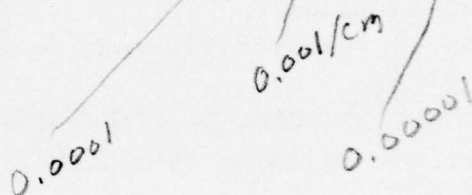
## UNCLASSIFIED

SECURITY CLASSIFICATION OF THIS PAGE(When Data Entered)

Block 20 (Abstract) cont'd.

micrometers

of electron microscopy, infrared absorption spectroscopy and transport property measurements were brought to bear on samples prepared here for this purpose. The third area of study included measurements of laser damage characteristics of IR window materials at both  $10.6\mu\text{m}$  and in the 2-5 $\mu\text{m}$  region. An effort to use surface acoustic waves to measure surface absorption was successfully completed during this period. A surface absorption as small as  $10^{-4}$  could be directly measured in the presence of a large bulk absorption,  $10^{-3}\text{cm}^{-1}$ . Analyses of this work suggest that surface absorptions as low as  $10^{-5}$  could be measured. This technology is being transferred to the China Lake Naval Weapons Center for refinement and extended use.



UNCLASSIFIED

SECURITY CLASSIFICATION OF THIS PAGE(When Data Entered)

(i)

## CONTENTS

### 1. Thermal Lensing Studies

- a) A Quantitative Experimental Investigation of Thermal Lensing\* (Christensen, Steier, Joiner)
- b) Measurement of Strain-optic Coefficients by Acousto-optic Interactions in Window Materials\* (Joiner, Steier, Christensen)
- c) Theory of Thermally Induced Birefringence in Polycrystalline Media (Flannery, Marburger)

### 2. Defect Studies

- a) An Electron Microscope Study of the Structural Imperfections in II-VI Compounds (CdTe and ZnSe) (Narayanan, Rustomji)
- b) Study of Defects in II-VI Compounds (Krøger, Selim, Ray)
- c) Absorption Studies of CdTe and ZnSe (Spitzer, Dutt)

### 3. Damage Studies

- a) High Power Infrared Damage Studies (Bass)
- b) The Dependence of the Pulsed  $10.6\mu\text{m}$  Laser Damage Threshold on the Manner in Which a Sample is Irradiated\*\* (Bass, Leung)

### 4. Surface Absorption Measurements

- a) Studies of Radiative Absorption at KC1 Surfaces Using Acoustic Techniques (Rockwell, Parks)
- b) Surface Acoustic Wave Velocity Dispersion Induced by Radiative Absorption (Parks, Rockwell)

\*Papers presented at Fifth Annual IR Window Conference

\*\*Paper published in IEEE Journ. Quant. Electron.

## INTRODUCTION

The projects described here fall under four broad subject areas: thermal lensing, defect properties, damage studies, and surface absorption measurements. Portions of this work have been reported at the Fifth Annual Conference on Infrared Laser Window Materials, Las Vegas, Dec. 1975. In some cases, technical details included in those conference proceedings are not repeated here. Nearly all the projects reported are related to work performed under a previous contract (F19628-75-C-0080), and the technical and final reports of that program include some background material on the projects described below.

A Quantitative Experimental Investigation  
of Thermal Lensing

C. P. Christensen, W. H. Steier, R. Joiner  
Department of Electrical Engineering  
University of Southern California  
Los Angeles, California 90007

Abstract

A quantitative comparison between experimental measurements and lensing theory in CdTe shows good agreement in both first order lensing and lens aberration.

Thermal lensing and optical distortion in infrared window materials have been treated theoretically by several investigators<sup>1</sup>, and qualitative agreement with theoretical predictions has been demonstrated experimentally in some cases.<sup>2</sup> However, a detailed, quantitative comparison of theory and experiment has not previously been reported and is necessary if composite window structures are to be designed to compensate for thermal lensing aberrations.

In this investigation thermal lensing experiments are conducted using a well characterized 50 watt CO<sub>2</sub> laser as the optical source and relatively high loss ( $\beta \sim 0.2 \text{ cm}^{-1}$ ) CdTe as the lensing medium. The laser operates in a fundamental TEM<sub>00</sub> Gaussian mode. Although the available laser power is not sufficient to induce measurable lensing in low loss materials, operation at the 50 watt level is desirable since parasitic distortion in beam-handling optics can be minimized, laser mode control is facilitated, and optical measurements are simplified at reduced power levels. The emphasis here is to obtain an experimental check on the theory of lensing and hence well characterized experimental conditions are stressed. The assumption is that the theory can be scaled to low loss materials and high laser powers which are of practical interest.

The lensing medium is uncompensated polycrystalline CdTe, 5 cm dia, by 1.3 cm thick; the relatively high loss is caused by free electrons. We assume

that these free carriers do not effectively change the material constants such as  $K$ , the heat conductivity;  $C_v$ , the heat capacity; and  $n$ , the index of refraction. We have calculated the effect of the free carriers on  $dn/dT$  and found the effect negligible.

The experimental setup is shown in Fig. 1 and uses a rotating mirror to scan the beam past a pinhole detector. The electronics shown enable us to select any scan up to 20 seconds after the sample is first illuminated. Typical results are shown in Fig. 2 for an incident laser power,  $P$ , of 25 W; for a sample to beam waist distance,  $L$ , of 1 m; and for a detector to sample distance,  $d$ , of 1 m. Fig. 2a is on a slow time scale and shows many scans to illustrate the build-up and decay of the on-axis intensity as the lensing develops. The individual scans clearly show the growth of the side lobes caused by the aberrations in the induced lens.

To compare these results with theory requires knowledge of the input Gaussian beam parameters. Figure 3 shows a slow scan of the input beam. From these scans taken at two distances from the laser, the position of the beam waist can be determined.<sup>3</sup> Our results show the waist to be 96 cm from the flat output mirror of the laser and a waist spot size radius of 2.4 mm. The theory for an empty optical cavity using the mirrors shown would predict the waist to be at the output mirror; the difference emphasizes the need for measurement of the beam parameters and is likely caused by lensing effects in the discharge tube. The beam parameters were found to be independent of the laser power output over the range of powers used in the experiments.

The calculations of the temperature profiles caused by the absorbed laser power were done by evaluating an exponential integral which is appropriate for an infinite media<sup>4</sup> and were also done by a difference equation technique which allows arbitrary radial boundary conditions. The solutions agreed well at times short compared to the thermal diffusion time to the sample boundary. Only radial heat flow was considered, since heat flow laterally off the sample surface was expected to be less than 1% of the radial heat flow.

The increase in absorption coefficient with temperatures due to the increase in free electron density was included in the temperature calculations and its effect on the infrared transmission of the sample was included in the diffraction calculation. The infrared absorption increases at about 3% per degree centigrade above room temperature.

The beam diffraction calculations used a scalar wave theory and assumed radial symmetry and a Gaussian input beam. The linear expansion of the sample with temperature was included and made an approximate 10% contribution to the lensing. The stress-optic effects were neglected, since the sample was polycrystalline, and this effect is expected to be small in CdTe. No resonant interference of the beams reflected from the sample surfaces<sup>5</sup> were considered since in the experiment the sample surfaces were not normal to the beam axis. We did, however, include the absorbed power from the first reflected beam inside the sample.

Figure 4 shows a typical comparison between the measurements and the theoretical calculations of the transmitted beam profiles. The theory is surprisingly good in predicting beam shapes but somewhat poorer in predicting absolute intensities, particularly at longer times. The agreement was in general this close with all of the data taken. The theory was found to be fairly sensitive to the values of material parameters used. In this comparison we used the best available values for CdTe ( $K = 0.07 \text{ W/cm}^2 \text{ }^\circ\text{C}$ ,  $C_v = 1.22 \text{ joule/cm}^3 \text{ }^\circ\text{C}$ ,  $dn/dT = 1.2 \times 10^{-4} / \text{ }^\circ\text{C}$ ).

In Figures 5, 6, 7, and 8 are plotted the on-axis intensity vs. time and the side lobe intensity vs. time for several experimental configurations. The theory fairly accurately predicts the on-axis intensity and correctly predicts the general trend of the side lobe intensity.

---

- <sup>1</sup> a) M. Sparks, J. Appl. Phys. 42, 5029 (1971)  
b) J. R. Jasperse and P. D. Gianino, J. Appl. Phys., 43, 1686 (1972)  
c) J. Marburger and M. Flannery, Conf. on High Power Laser Window Materials, AFCRL - 71 - 0592, Special Report No. 127 (1971)
- <sup>2</sup> a) L. H. Skolnik, B. Bendow, and E. F. Cross, Appl. Optics 13, 726 (1974)  
b) B. Bendow, L. H. Skolnik, E. F. Cross, Appl. Optics 13, 729 (1974)
- <sup>3</sup> H. Kogelnik and T. Li, Appl. Optics 5, 1550 (1966)
- <sup>4</sup> J. Gordon, K. Leite, R. Moore, S. Porto, and J. Whinnery, J. Appl. Phys. 36, 3 (1965)
- <sup>5</sup> B. Bendow, L. H. Skolnik, E. F. Cross, Appl. Optics 13, 729 (1974)

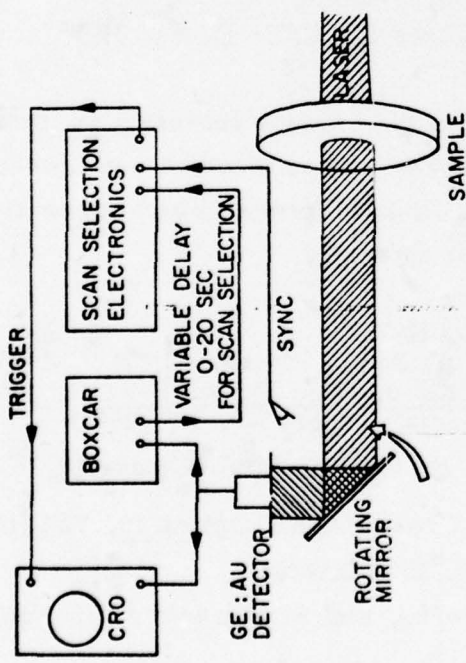


Fig. 1

SLOW SCAN OF LASER MODE

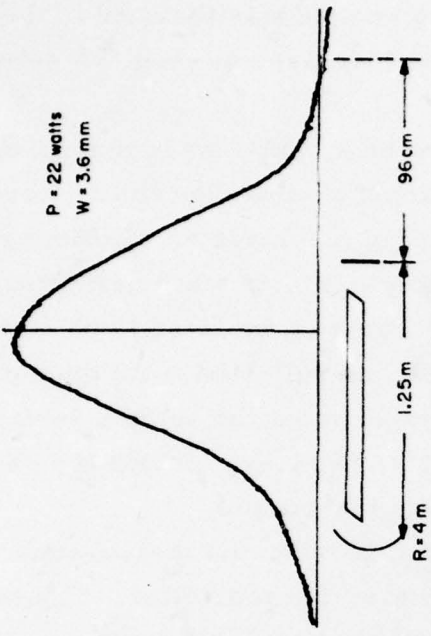


Fig. 3

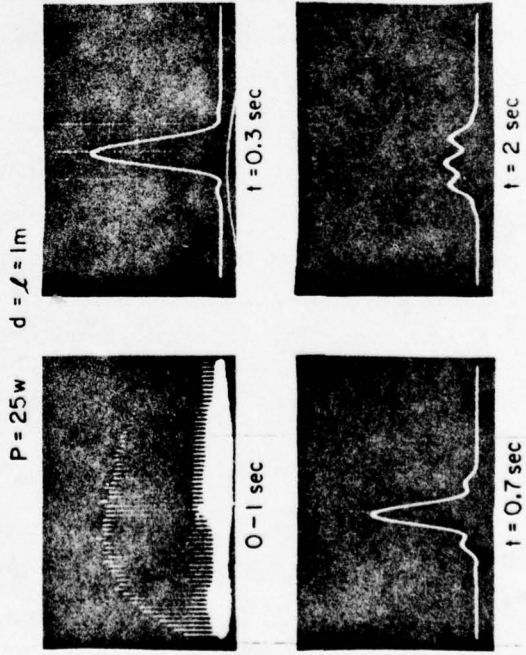


Fig. 2

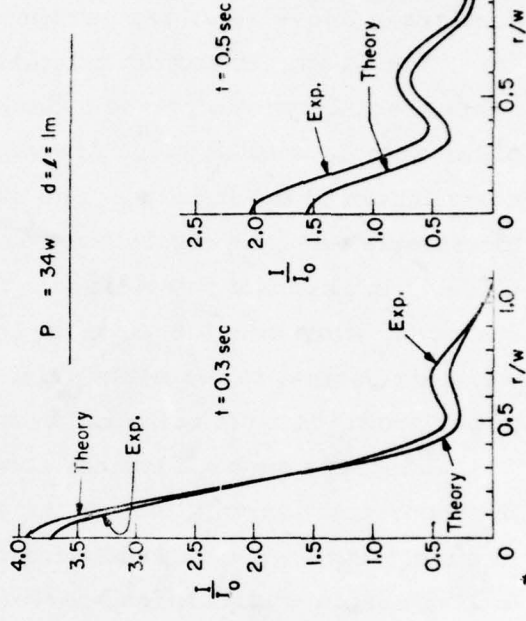


Fig. 4

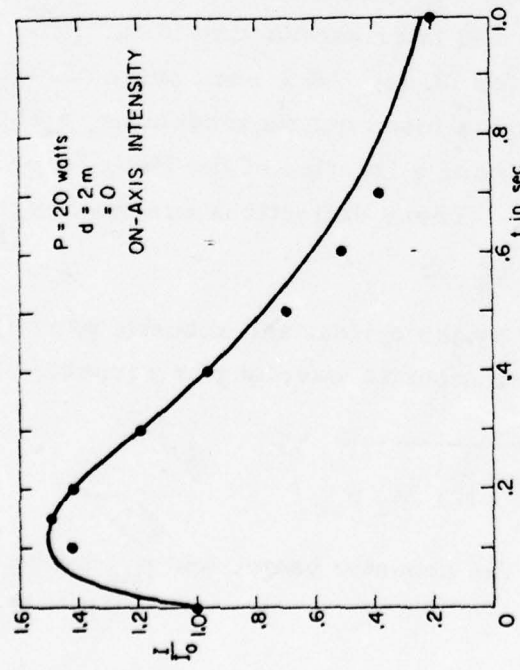


Fig. 5

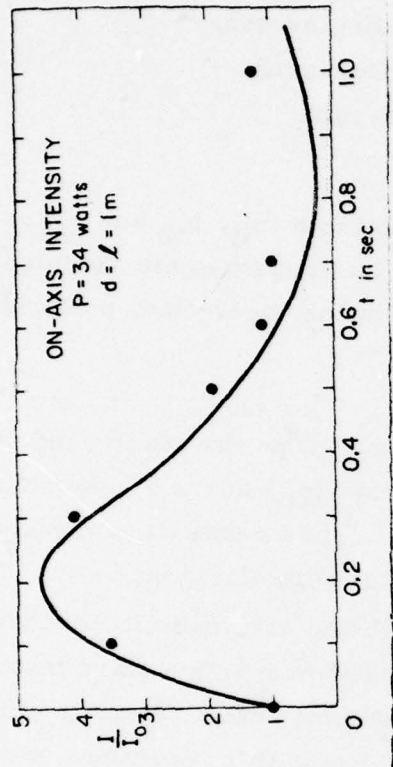


Fig. 7

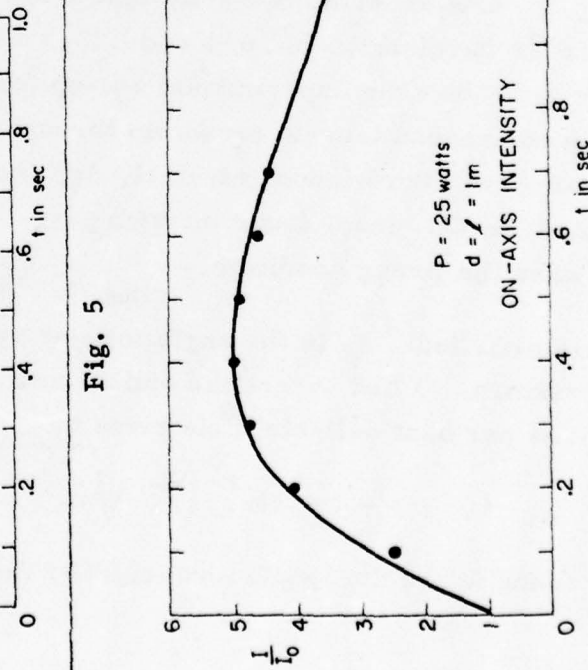


Fig. 6

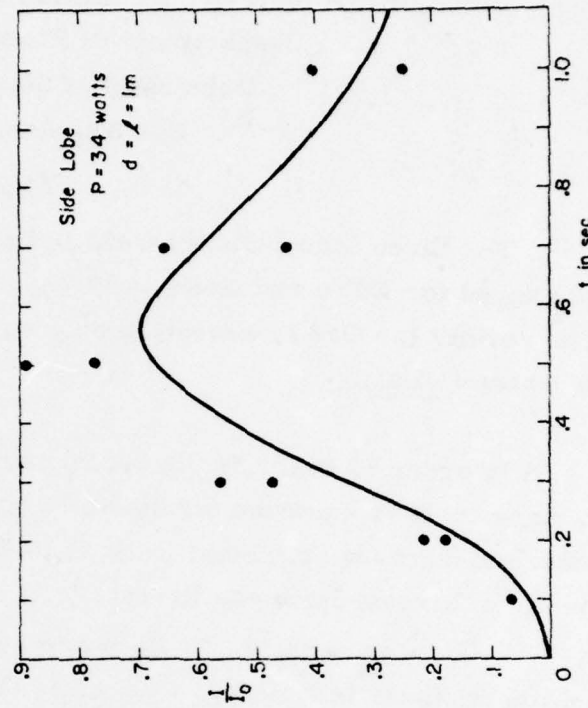


Fig. 8

Measurement of Strain-Optic Coefficients  
By Acousto-Optic Interactions in Window Materials  
R. Joiner, W. H. Steier, and C. P. Christensen  
Department of Electrical Engineering  
University of Southern California  
Los Angeles, California

Abstract

The three independent strain-optic coefficients ( $p_{11}$ ,  $p_{12}$  and  $p_{44}$ ) were measured for CdTe and GaAs at  $10.6\mu$ , using an acousto-optic technique. The results for GaAs, excepting  $p_{12}$ , agree with the theoretical predictions of Bendow *et al.*

In order to evaluate the performance of a high power laser window, it is necessary to know the strain-optic coefficients ( $p_{ij}$ ) of the window materials.<sup>1</sup> Recent experimental work at  $10.6\mu$ <sup>2, 3, 4</sup> has resulted in measurements of stress-optic coefficients ( $q_{ij}$ ) and stress-birefringence coefficients ( $c_\lambda = \frac{n}{2} (q_{11} - q_{12})$ ). Both are related to the strain-optic coefficients by the stiffness tensor ( $p_{ij} = q_{ik} c_{kj}$ ). This paper presents a third method which was originally devised to measure strain-optic coefficients in candidate materials for acousto-optic modulators. Using this technique, we were able to determine all three independent coefficients for both GaAs and CdTe.

The experimental technique was first demonstrated by Dixon<sup>5, 6</sup> at laser wavelengths of  $.63\mu$  and  $1.15\mu$  and later extended to  $10.6\mu$ <sup>7, 8</sup>. Figure 1 shows the experimental set-up for  $10.6\mu$ . A  $2\ \mu$ sec pulse of high frequency sound travels roundtrip through a fused quartz modulator, a salol bond, and the window material, deflecting a fraction of the HeNe laser beam and the  $\text{CO}_2$  laser beam on each pass. These deflections are maximized when the Bragg condition

$$\sin\theta_B = \frac{\lambda}{2\Lambda} \quad (1)$$

is satisfied.<sup>9</sup>  $\theta_B$  is the angle formed by the optical and acoustic propagation vectors.  $\lambda$  and  $\Lambda$  are the optical and acoustic wavelengths respectively.

The per cent deflected<sup>10</sup> is given by

$$\frac{I}{I_0} = \sin^2 \left( \frac{\pi}{2} \sqrt{\frac{2}{\lambda^2} \left( \frac{L}{H} \right) M_2 p_{ac}} \right) \quad (2)$$

$L$  and  $H$  are the length and height of the acoustic beam, and  $p_{ac}$  is the acou-

stic power. The acousto-optic figure of merit,  $M_2$ , is a function of the index of refraction,  $n$ ; the density,  $\rho$ ; the acoustic velocity,  $V$ ; and the appropriate strain-optic coefficient,  $p$ .

$$M_2 = \frac{n^6}{\rho} \frac{p^2}{V^3} \quad (3)$$

Note that in equation (2) a longer wavelength implies smaller deflections for a given figure of merit.

Simply solving equation (2) for  $M_2$  requires a knowledge of the acoustic power, which is a function of acoustic losses in the material and the quality of the salol bond. By assuming small deflections and taking ratios of the deflected pulses shown in Figure 2, a simple formula relating  $M_2$  to a known figure of merit for quartz can be derived and does not require a knowledge of the acoustic power.

$$\frac{M_2 \text{ (sample)}}{M_2 \text{ (quartz)}} = \left( \frac{I_4 I_5}{I_1 I_3} \right)^{\frac{1}{2}} \left( \frac{10.6\mu}{0.633\mu} \right)^2 \quad (4)$$

For GaAs and CdTe, there are only three independent strain-optic coefficients,  $p_{11}$ ,  $p_{12}$ , and  $p_{44}$ . For longitudinal sound propagating along a  $\langle 100 \rangle$  direction, we can measure  $p_{11}$  by using light polarized parallel to the plane containing the light and sound propagation vectors, and we can measure  $p_{12}$  by using a light polarization perpendicular to that plane. For sound propagating along a  $\langle 111 \rangle$  direction, the two polarizations yield

$$p'_{11} = \frac{1}{3} (p_{11} + 2p_{12} + 4p_{44}) \quad (5)$$

$$p'_{12} = \frac{1}{3} (p_{11} + 2p_{12} - 2p_{44}) \quad (6)$$

$p_{44}$  is then calculated either by subtracting equation (6) from equation (5) or by substituting  $p_{11}$  and  $p_{12}$  into either equation (5) or (6). Since strain-optic coefficients can be either positive or negative, a separate, but simple experiment must be done to determine relative signs.<sup>8</sup>

Some care and compromises are required to assure that the experimental conditions are appropriate with the assumptions inherent in equation (4). Equation (4) is valid for small deflections and for acoustic frequencies

near those defined by the Bragg regime<sup>9</sup>. It is also necessary that the IR beam divergence be less than the acoustic beam divergence<sup>11</sup>. In our case, we were able to use an acoustic frequency and to adjust the IR beam size to reasonably meet these requirements. However, this resulted in the sound pulse's interacting at any one time with only a portion of the IR beam, which produced a deflected IR pulse longer and of lower intensity than was expected. To account for this, a boxcar integrator was used to measure the integrated deflected intensity.

Samples of CdTe and GaAs oriented  $\langle 100 \rangle$  and  $\langle 111 \rangle$  were measured, and the results of those measurements are shown in Table I. The GaAs samples were measured at an acoustic frequency of 150 MHz, and the CdTe was measured at 50 MHz. Figure 3 shows a comparison of experimental (circles) and theoretical (solid lines) values for GaAs. The values at  $1.15\mu$  were measured by Dixon<sup>6</sup>. The theory of Bendow *et al.*<sup>12</sup> extended these results to longer wavelengths and predicted little change at  $10.6\mu$ . Experimental results concur, with the exception of  $p_{12}$ .

In an attempt to measure polycrystalline ZnSe, it was found that the grain sizes were of the order of an acoustic wavelength and no coherent interaction between light and sound was observed past a few millimeters into the ZnSe.

This method offers some advantages over birefringence or interferometric methods in that i) since the strain is an acoustic traveling wave, the difficulties of applying a uniform strain to the sample and of residual strain in the sample are avoided; ii) the stability of an interferometer is not required; and, iii) all three coefficients for cubic materials are measured. However, the signal in this method tends to be small since it is proportional to  $p^2$  while in the interferometer method the signal is proportional to  $p$ .

### References

1. M. Sparks, *J. Appl. Phys.*, 42, 5029 (1971).
2. A. Feldman, I. H. Malitson, D. Horowitz, R. M. Waxler and M. J. Dodge, *Proceedings of the Fourth Annual Conference on IR Laser Window Materials*, Nov. 1974, compiled by C. R. Andrews and C. L. Strecker, p. 118.
3. J. C. Corelli and J. P. Szcześniak, *Proceedings of the Fourth Annual Conference on IR Laser Window Materials*, Nov. 1974, compiled by C. R. Andrews and C. L. Strecker, p. 132.
4. C. A. Pitha and J. D. Friedman, *Proceedings of the Fourth Annual Conference on IR Laser Window Materials*, Nov. 1974, compiled by C. R. Andrews and C. L. Strecker, p. 149.
5. R. W. Dixon and M. G. Cohen, *Appl. Phys. Letters* 8, 205 (1966).
6. R. W. Dixon, *J. Appl. Phys.*, 38, 5149 (1967).
7. R. W. Dixon and A. N. Chester, *Appl. Phys. Letters* 9, 190 (1966).
8. R. L. Abrams and D. A. Pinnow, *J. Appl. Phys.* 41, 2765 (1970).
9. R. Adler, *IEEE Spectrum*, 42, May 1967.
10. D. A. Pinnow, *IEEE J. Quantum Electronics*, Vol. QE-6, 223, April 1970.
11. E. I. Gordon, *Proc. IEEE*, Vol. 54, 1391, October 1966.
12. B. Bendow, P. D. Gianino, S. S. Mitra, and Y. Tsay, *Third Conference on High Power IR Laser Window Materials*, Nov. 1973, edited by C. A. Pitha and B. Bendow, p. 367.

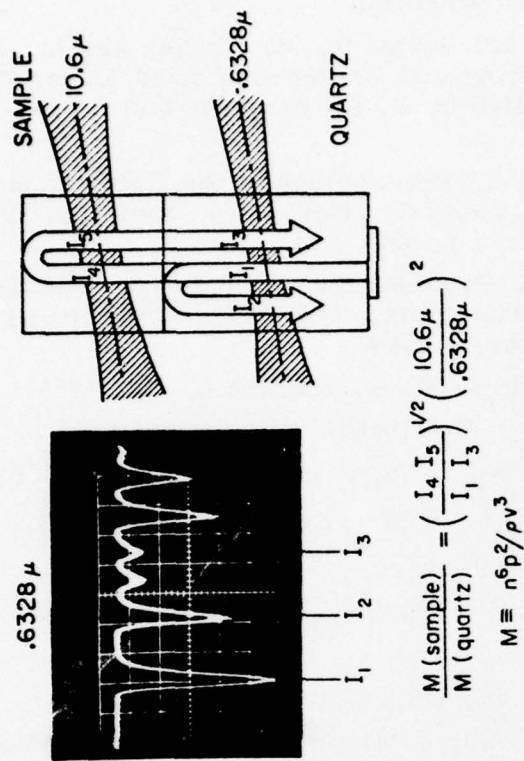


Fig. 1

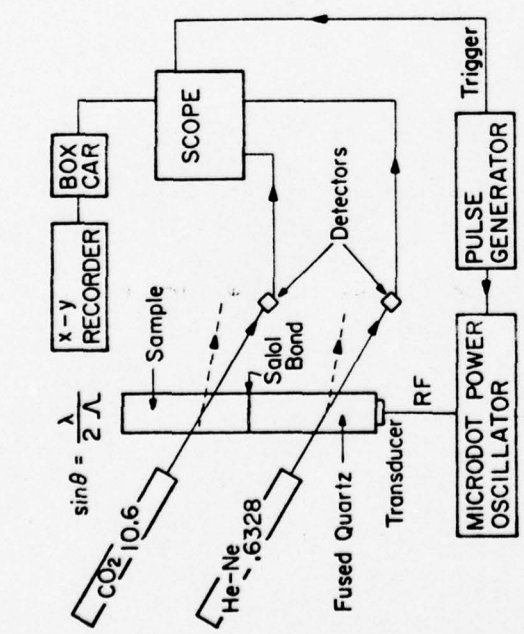


Fig. 2

$$\frac{M(\text{sample})}{M(\text{quartz})} = \left( \frac{I_4 I_5}{I_1 I_3} \right)^{1/2} \left( \frac{10.6\mu}{6.328\mu} \right)^2$$

$$M \equiv n^6 p^2 / \rho v^3$$

10.6 μ  
6.328 μ  
SAMPLE  
QUARTZ

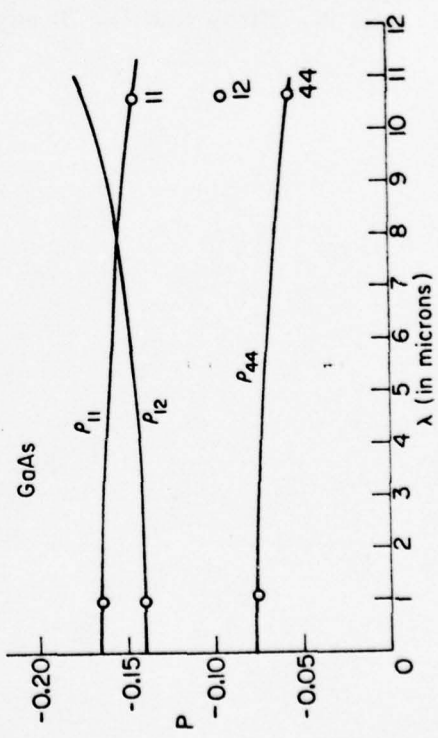


Fig. 3

Table 1

Theory of Thermally Induced Birefringence in Polycrystalline Media

M. Flannery, J. H. Marburger

During the initial period of this contract, we developed what promises to be an accurate theory of stress induced birefringence in polycrystalline media. This theory, which is based on work of Hershey and Dahlgren<sup>1</sup> on the elastic properties of polycrystalline media, was reported at the Fifth Annual Conference on IR Window Materials<sup>2</sup> and also published as an Applied Physics Letter.<sup>3</sup>

The result of this theory is an expression for the components of the effective strain optic tensor  $p_{ij}^*$  of an ideal polycrystalline material in terms of the single crystal values of the tensor components  $p_{ij}$  and of the elastic coefficients  $c_{ij}$ . The theory has been developed only for materials of cubic symmetry of the classes  $\bar{4}3m$ ,  $432$  and  $m3m$ , which include all the currently interesting IR window materials. For these classes, only the tensor components  $p_{11}$ ,  $p_{12}$ ,  $p_{44}$  are nonvanishing. (We use the usual 6 dimensional matrix notation for the symmetric tensors  $p_{ijkl}$ ,  $c_{ijkl}$ , etc.) The main results of the theory are:

1. The combination  $(p_{11}^* + 2p_{12}^*)/3$  is equal to the single crystal expression  $(p_{11} + 2p_{12})/3$ , and the elastic coefficients also obey this relation:

$$(c_{11}^* + 2c_{12}^*)/3 = (c_{11} + 2c_{12})/3 = \kappa = \text{bulk modulus.}$$

2. The combination  $p_{11}^* - p_{12}^*$  satisfies

$$\frac{p_{11}^* - p_{12}^*}{2\mu} = \frac{p_{11} - p_{12}}{c_{11} - c_{12}} + \psi \left[ \frac{p_{44}}{c_{44}} - \left( \frac{p_{11} - p_{12}}{c_{11} - c_{12}} \right) \right]$$

where  $\mu = \frac{1}{2}(c_{11}^* - c_{12}^*)$  and

$$\psi = \frac{3(3\kappa + 4\mu)c_{44}}{(9\kappa + 8\mu)\mu + 6(\kappa + 2\mu)c_{44}}.$$

3. The effective shear modulus  $\mu$  of the polycrystalline medium is the only positive root of a quartic equation whose coefficients depend upon  $c_{11}$ ,  $c_{12}$  and  $c_{44}$ . The value of  $\mu$

determined from this equation falls between the Hashin-Shtrikman bounds, which are derived from very general considerations.<sup>4</sup>

Having determined  $p_{ij}^*$ , it is necessary to compare the performance of a polycrystalline window with that of a single crystal window. This is not easy because, even for cubic materials, an arbitrarily oriented window does not possess sufficient symmetry in the window plane to allow an analytical solution of the thermal stress problem. Only in one case is the analysis tractable: When the window is parallel to a (111) plane, the relation between stress and strain in the plane stress approximation has the same tensor form as that for isotropic media, and closed expressions can be obtained for the strain in a nonuniformly heated window. This configuration was treated by F. Horrigan (private communication) and also by us, and the results were reported in the Fourth Annual IR Window Conference proceedings.<sup>5</sup>

The results for a (111) window can be summarized as follows: The induced birefringence effects are described by the difference  $2\Phi$  between the phases of radial and azimuthal polarization components of the incident optical field. (We are assuming a circularly symmetric intensity distribution, centered on a self-constrained edge-cooled window.) In the short pulse heating regime, where thermal conductivity does not distort the temperature distribution, the phase may be written simply as

$$\Phi = F[g(r) - 2f(r)]$$

where  $f(r)$  and  $g(r)$  are related to the incident beam shape. For a gaussian beam with  $1/e$  intensity radius  $a$ ,

$$f(r) = \exp(-r^2/a^2)$$

$$g(r) = [1 - \exp(-r^2/a^2)]/(r^2/2a^2).$$

The dimensionless parameter  $F$  is

$$F = \frac{\beta I_0 t \alpha n^3 \kappa}{2c'} \left\{ \frac{c_{44}(c_{11} - c_{12})}{2c_{11}c_{44} + 3\kappa(c_{11} - c_{12})} \left[ \frac{p_{11} - p_{12}}{c_{11} - c_{12}} + \frac{2p_{44}}{c_{44}} \right] \right\}$$

where  $\beta$  = absorption coefficient

$I_0$  = axial incident intensity

$t$  = illumination time

$L$  = window thickness

$\alpha$  = thermal expansion coefficient

$n$  = window refractive index

$\kappa$  = bulk modulus

$c'$  = volume specific heat.

In the isotropic limit  $c_{44} \rightarrow c_{44}^* = \frac{1}{2}(c_{11}^* - c_{12}^*)$ ,  
 $p_{44} \rightarrow p_{44}^* = \frac{1}{2}(p_{11}^* - p_{12}^*)$ , we have

$$F_{pc} = A \left\{ \frac{9}{8} \frac{(p_{11}^* - p_{12}^*)}{(3\kappa + \mu)} \right\}$$

where  $A$  is the factor multiplying the curly brackets. Prior to the development of a polycrystalline theory, the birefringence contribution was estimated by<sup>6</sup>

$$F_0 = A \left\{ \frac{9}{8} \frac{(p_{11} - p_{12})}{(3\kappa + \mu)} \right\}$$

where  $p_{11}$  and  $p_{12}$  are single crystal parameters.

In Table I, we list the values of  $F/A$ ,  $F_{pc}/A$ , and  $F_0/A$ . The better figure should no longer be used as a figure of merit. The others are proportional to figures of merit for (111) single crystal windows and for polycrystalline windows, respectively.

We conclude from Table I that the estimates of the earlier crude theory are closer in magnitude to the polycrystalline results, although the predicted sign of the effect is frequently incorrect. In passing from (111) single crystal to polycrystal, the magnitude of the birefringence is reduced by up to a factor of ten, but the sign is not changed. In the important cases of  $\text{CaF}_2$  and  $\text{BaF}_2$ , the correct polycrystalline values are respectively factors of 2 and 3 greater than the previous estimate, although the polycrystalline forms of these materials still have respectively 9 and 5 times less birefringence than the

(111) single crystal.

Table I. Thermally induced birefringence parameters for windows fabricated from materials with cubic symmetry in their crystalline form.

Material	$F_o/A$	$F/A$	$F_{pc}/A$
NaCl	- .00532	- 0.0199	- 0.00346
KCl	.00932	- 0.0668	- 0.00412
KBr	.0104	- 0.0684	- 0.00396
CaF <sub>2</sub>	- .0255	0.420	0.0470
BaF <sub>2</sub>	- .0191	0.286	0.0555
GeP	- .00241	- 0.0132	- 0.00387
GeAs	- .00104	- 0.0122	- 0.00365
Ge	.00140	0.0223	0.00605
Diamond	- .00375	- 0.0130	- 0.00272

The table entries are proportional to the phase difference introduced between radial and azimuthal polarization components of the incident optical field.  $F_o/A$  is the approximation used previously to estimate the magnitude of the effect.  $F/A$  is the exact value for a (111) single crystal window.  $F_{pc}/A$  is the theoretical value for an ideal polycrystalline window.

Our next task is to determine whether partial orientation of the grains can reduce the birefringence still further. This investigation requires a modification of the entire Hershey-Dahlgren model of polycrystalline materials, and is now in progress.

#### References:

1. A.V. Hershey, V.A. Dahlgren, Journ. App. Mech. 21, 236 (1954).
2. M. Flannery, J. Marburger, in Proceedings of the Fifth Annual Conference on IR Window Materials, ed. by C.R. Andrews and C.L. Strecker, Feb. 1976.
3. M. Flannery, J. Marburger, Appl. Phys. Lett. 28, 600 (1976).

4. Z. Hashin, S. Shtrikman, J. Mech. Phys. Solids 10, 343 (1962).
5. B. Bendow, Peter D. Gianino, M. Flannery and J. Marburger, in Proceedings of the Fourth Annual Conference on IR Window Materials.
6. B. Bendow, Peter D. Gianino, Appl. Phys. 2, 1 (1973); 2, 71 (1973).

An Electron Microscope Study of the Structural Imperfections in II-VI Compounds (CdTe and ZnSe)

G.H. Narayanan and S.H. Rustomji

The goal of this part of the research program is to identify and characterize the lattice defects and other structural inhomogenieties in CdTe and ZnSe by using transmission electron microscopy techniques. The work in this period was concentrated on the study of P-doped CdTe. The electrical and optical properties of this material have been also investigated in our laboratories by Professor Kroger's group and by Professor Spitzer's group respectively.

It is known that the native defect centers, impurities and precipitates control the electrical and optical properties of CdTe and that the precise nature and concentrations of these defects are dependent on the crystal growth conditions and post-growth annealing treatments. In the present investigation, therefore, it was proposed to examine the defect substructure of CdTe:P crystals in the as-grown condition as a function of the P concentrations and further to investigate how the defect structure was influenced by post-growth annealing treatments under well-defined partial pressures of Cd and Te. Also, attempts were made to correlate the results of the present studies with the electrical and optical properties measurements carried out here at USC on materials of identical chemical composition and thermal history.

CdTe ingots with P concentrations of  $5 \times 10^{19}$ ,  $5 \times 10^{18}$ ,  $2 \times 10^{17}$  and  $5 \times 10^{16} \text{ cm}^{-3}$  were grown from melt by the horizontal Bridgman technique in our laboratory by Dr. B.V. Dutt. No attempt was made to control the over-pressure during crystal growth. Samples were cut from each ingot and annealed at  $700^\circ\text{C}$  under Cd partial pressures of  $2.4 \times 10^{-5}$ ,  $1 \times 10^{-3}$ ,

$1 \times 10^{-2}$ ,  $1 \times 10^{-1}$  and  $2 \times 10^{-2}$  atms. for periods of time long enough to achieve equilibrium. All the samples were quenched to room temperature following heat treatments. Both as-grown and annealed samples were first mechanically ground from both surfaces to produce wafers  $\sim 200\mu$  in thickness and subsequently cut into specimens  $3 \times 3$  mm in size. Final thinning to obtain electron transparent specimens was done by a chemical jet polishing technique described previously (1).

Fig. 1 (a) through (c) shows typical bright field micrographs of CdTe:P crystals in the as-grown condition for P concentrations of  $5 \times 10^{19}$ ,  $5 \times 10^{18}$ , and  $5 \times 10^{16} \text{ cm}^{-3}$  respectively. Evident in these micrographs is the presence of fine precipitates, approximately  $100-200 \text{ \AA}$  in size, distributed uniformly throughout the matrix. The density of the precipitate is higher in crystal with higher P content. Since no diffraction effects attributable to the precipitate appeared in the electron diffraction patterns, a positive identification of the nature of the precipitate phase could not be made. However, the apparent dependence of the density of precipitates on P content suggests that the precipitates might be some compound involving P. There are two known phosphorous compounds in the Cd-Te-P system,  $\text{Cd}_3\text{P}_2$  and  $\text{P}_2\text{Te}_3$ , which are worth considering. In the present case the precipitates are more likely to be those of  $\text{Cd}_3\text{P}_2$  if we consider the fact that P was introduced into the crystal through additions of  $\text{Cd}_3\text{P}_2$  into the melt during crystal growth. The formation of these compounds have been speculated also by Hall and Woodbury<sup>(2)</sup> in their investigations of the diffusion and solubility of P in CdTe.

Apart from the precipitates the as-grown crystals were virtually free of other types of defects such as voids which result from the condensation of excess vacancies as has been observed in some vapous grown CdTe<sup>(3)</sup>. The average dislocation density in all the crystals studies was well below  $10^4/\text{cm}^2$ .

### Defects in Annealed Crystals

Fig. 2 (a) through (d) shows typical microstructures of CdTe specimens with  $[P] = 5 \times 10^{19} \text{ cm}^{-3}$  following annealing at  $700^\circ\text{C}$  under progressively higher Cd partial pressures  $-2.4 \times 10^{-5}$ ,  $2 \times 10^{-3}$ ,  $1 \times 10^{-1}$  and  $2 \times 10^{-1}$  respectively. It can be seen that at the lowest Cd pressure (Te partial pressure) the microstructure reveals the presence of a moderately high density of voids distributed uniformly throughout the matrix. A careful examination of these voids shows that in many cases they are partially filled with a second phase (indicated by the arrows). These voids are polygonal in shape and range in size from 700 to  $1200 \text{ \AA}$ . Their number density is  $\sim 5 \times 10^{13} / \text{cm}^3$ . The origin of these partially filled voids can be understood on the basis of the mechanism proposed by Shiozwa et al.<sup>(4)</sup>. It has been pointed out that annealing under Te over-pressures (i.e. very low Cd pressure) could lead to the presence of equilibrium concentration of Cd vacancies that are in excess of Te vacancies at the annealing temperature. On cooling to room temperature, the Cd vacancies coalesce into microscopic voids, with the Te atoms which would normally occupy the lattice sites in that region of the crystal partially filling this void. This type of voids have been previously observed in vapour grown CdTe<sup>(3)</sup>.

In specimens annealed under a Cd pressure of  $2 \times 10^{-3}$  atms there was a slight decrease in the volume fraction of the voids. In this specimen, however, there were essentially two different distributions of void sizes - a few large partially filled voids of size  $500-1400 \text{ \AA}$  coexisting with a fairly uniform distribution of large numbers of extremely fine voids  $100-150 \text{ \AA}$  in size were found to exist as shown in Fig. 1 (b). The matrix regions adjacent to the larger voids were found to be virtually free of the smaller voids. In many cases the larger voids were found to be preferentially

nucleated on matrix dislocations. The origin of these two distinctly different size distributions of voids is not clearly understood at the present time. In addition to the voids, a high density of precipitates can also be seen in this microstructure. Annealing under still higher partial pressures of Cd, did not result in the formation of any identifiable voids. However a distribution of fine precipitates was observed in specimens annealed at Cd partial pressure of  $1 \times 10^{-1}$  atm. but not at  $1 \times 10^{-2}$ . An example of this precipitation is shown in Fig. 2 (c). At the highest Cd partial pressure used in this study, namely 0.2 atms, the formation of a few voids were again observed. These voids, in general, were found to be tetrahedral in shape and nucleated predominantly on the matrix dislocations. They are believed to be due to the condensation of vacancies of tellurium.

In addition to Cd partial pressure, the total concentration of [P] in the crystal was also found to have a pronounced effect on the substructure of annealed crystals. When annealing was carried out at very low Cd partial pressure viz:  $2.4 \times 10^{-5}$  atm., the volume fraction of the void-precipitate complex was found to decrease progressively with decreases in P content as shown in Fig. 3 (a) and (b). At a  $p_{Cd}$  of  $1 \times 10^{-3}$  atms voids were still observed in all crystals, except the one with the lowest P content, namely  $10^{16} \text{ cm}^{-3}$ . However the void volume fraction was consistently lower than those observed in crystals under low  $p_{Cd}$ . At intermediate partial pressure i.e.  $1 \times 10^{-2}$  atms, precipitates 100-300 Å in size were observed in crystals containing  $2 \times 10^{17}$  and  $6 \times 10^{16} \text{ P/cm}^{-3}$ . Crystals with higher P concentrations were virtually free of any defects following this heat treatment. Fig. 4 (a) and (b) show typical microstructures of crystals with  $2 \times 10^{17}$  and  $6 \times 10^{16} \text{ cm}^{-3}$  of P respectively following annealing under a  $p_{Cd} = 1 \times 10^{-2}$  atms. Annealing at higher Cd pressures, 0.1 atms;

produced materials which exhibited little or no precipitation when P concentration was either  $2 \times 10^{18}$  or  $2 \times 10^{17} \text{ P/cm}^3$ . While small amounts of precipitated phase was observed in crystals with  $6 \times 10^{16} \text{ P/cm}^3$  and  $5 \times 10^{19} \text{ P/cm}^3$ .

The results of the present electron microscopy studies are, in general, consistent with the defect model proposed by Selim and Kroger<sup>(5)</sup> based on their results of Hall effect measurements and previous diffusion and solubility measurements of Hall and Woodbury<sup>(2)</sup>. Using the data presented by Selim and Kroger it is possible to construct defect isotherms valid for 700°C, in which the concentrations of the defects dominant in the neutrality conditions are plotted as a function of the P concentration for various Cd over pressure. The effects of  $p_{\text{Cd}}$  and total P content of the crystal on the annealed microstructures can be satisfactorily explained on the basis of these isotherms. At very low Cd partial pressures, i.e.:  $2.4 \times 10^{-5}$  atms the isotherm predicts Cd-vacancies  $V'_{\text{Cd}}$ , as the predominant defect, the concentration of which is estimated to be of the order of  $10^{18} \text{ /cm}^3$  for crystals with  $5 \times 10^{19} \text{ /cm}^3$  of P. When these crystals are cooled to room temperature, coalescence of the excess Cd vacancies can occur leading to formation of voids, half filled with Te atoms which would normally occupy the lattice site in that region. At a  $p_{\text{Cd}}$  of  $10^{-3}$  atms the isotherms predict a much lower  $V'_{\text{Cd}}$  concentration at all P concentration, thus accounting for the decrease in void volume fraction. The isotherm also shows that when total concentration exceeds  $10^{18} \text{ /cm}^3$ ,  $P'_i$  becomes a dominant defect species, their concentrations being of the order of  $10^{18} \text{ /cm}^3$  in crystals with  $10^{19} \text{ P/cm}^3$ . Precipitation of these interstitial P can occur during cooling to room temperature, which would explain the presence of precipitates in crystals with  $10^{18}$  and  $10^{19} \text{ P/cm}^3$ . For  $p_{\text{Cd}}$  equal to or greater than  $10^{-2}$  atms  $V'_{\text{Cd}}$  is no longer a dominant defect species at

all P concentrations. Consequently no voids are to be expected, in agreement with experimental observations. However the isotherm shows at this  $p_{\text{Cd}}$ ,  $P_i$  to be the dominant defect in crystals with P contents of  $6 \times 10^{16}$  and  $2 \times 10^{17} / \text{cm}^3$ . For P concentrations of  $10^{18}$  and  $10^{19} / \text{cm}^3$ ,  $P_i$  was found to form neutral complexes with  $P_{\text{Cd}}$ . Based on these isotherms one can predict that the precipitation of  $P_i^+$  might occur in crystals with  $10^{16}$  and  $10^{17} [\text{P}]$  and little or no precipitation in crystals with higher P content. This is in agreement with the electron microscopy observation. When annealed under a  $p_{\text{Cd}}$  of  $10^{-1}$  atms, the defect isotherms show  $\text{Cd}_i^{++}$  as a dominant defect species in crystals with P content up to  $\sim 10^{18} / \text{cm}^3$ ; beyond this, the formation of  $(\text{P}_{\text{Cd}} 2\text{P}_i)^*$  complexes are predicted. According to this model therefore, precipitates are predicted in the annealed crystals at lower P concentrations which is what was observed in the microstructure. It should be pointed out that distinction between precipitates of  $P_i$  and  $\text{Cd}_i^{++}$  are difficult under the present condition owing to the absence of any detectable diffraction effects due to these precipitate phases in the electron diffraction patterns.

During the remainder of the contract period we propose to carry out the following studies:

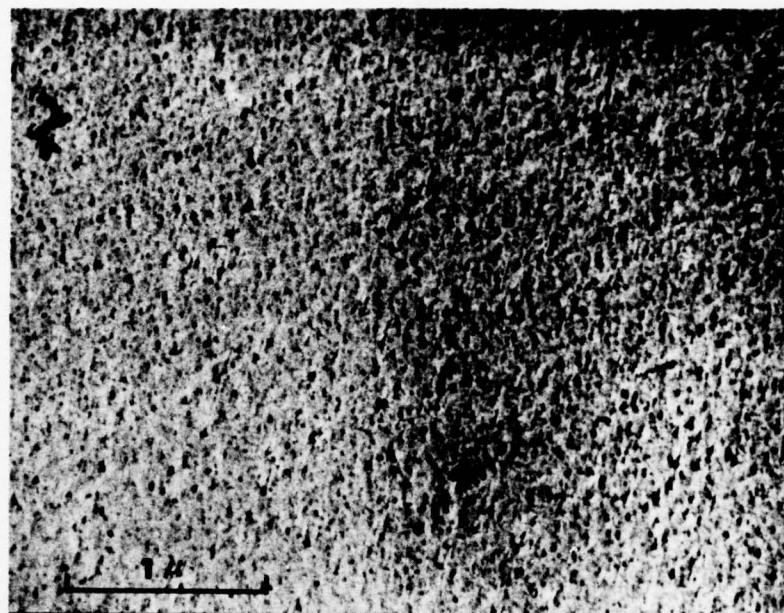
- (i) an investigation of the microstructures of CdTe doped with Ge both in the as-grown and annealed conditions.
- (ii) an investigation of the microstructural characteristics of ZnSe, doped with various concentrations of Al following various annealing treatments.

The electrical and optical properties measurements on these materials have been carried out here at USC by Professor Kroger and his students. An attempt will be, therefore, made to correlate the microstructural features with the measured physical properties.

## References

1. G.H. Narayanan and S.H. Rustomji: I.R. Window Studies Semi-Annual Technical Report #2 AFCRL-TR-75-
2. R.B. Hall and H.H. Woodbury: J. Appl. Phys. 39, 5361 (1968).
3. E.L. Hall, J.B. Vander Sande, P.J. Lamaure: Proc. of Fourth Conference on High Power Infrared Laser Window Materials; Defense Advanced Research Projects Agency. Arlington, VA, Jan. 1975 p. 531.
4. L.R. Shiozawa, J.M. Jost and D.A. Roberts, Proc. of Third Conference on High Power Infrared Laser Window Materials; Edited by Carl Pitha, Volume II 639 (1972).
5. F.A. Selim and F.A. Kroger, "The Defect Structure of Phosphorous-Doped CdTe" to be published.

(a)



$5 \times 10^{19} \text{ P/cm}^3$

As-grown CdTe:P



$2 \times 10^{18} \text{ P/cm}^3$

(b)



$6 \times 10^{16} \text{ P/cm}^3$

(c)

FIG·1

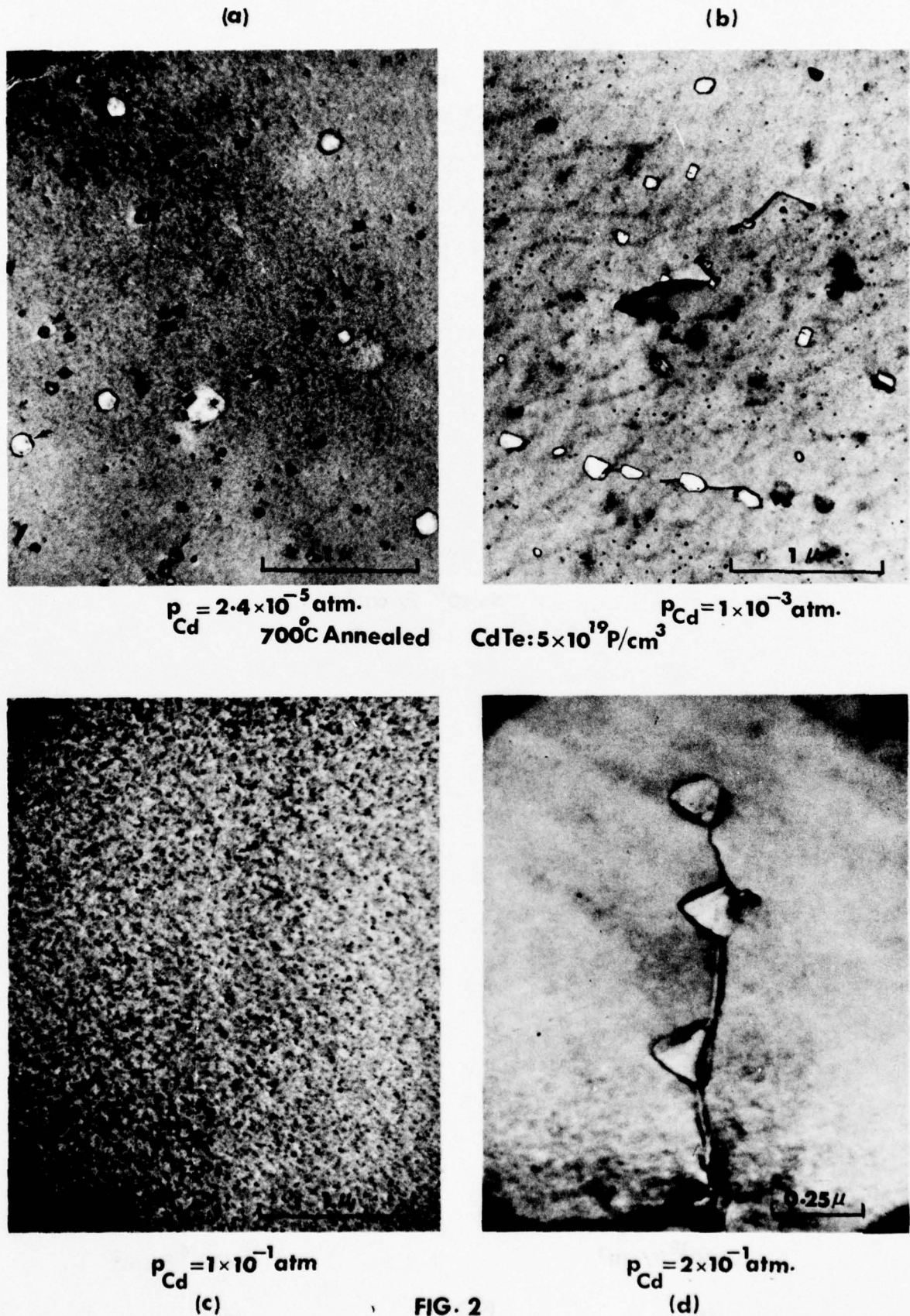
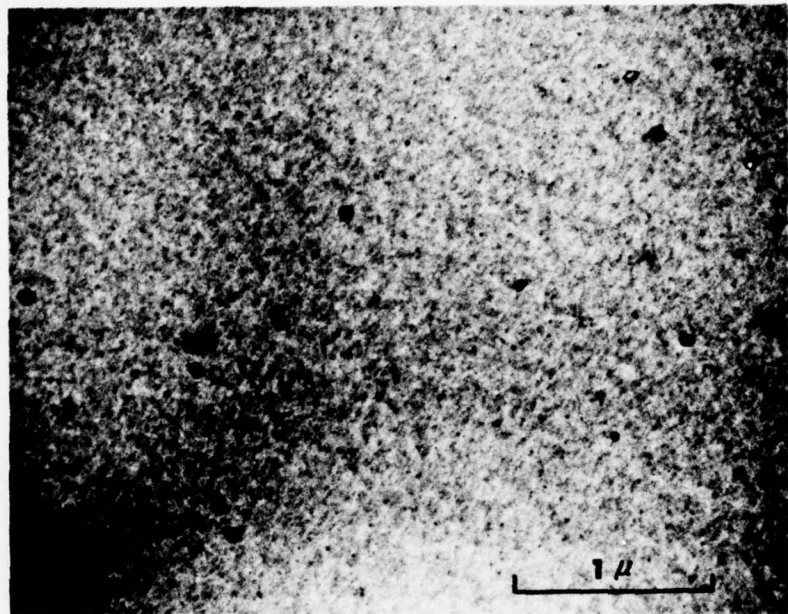


FIG. 2

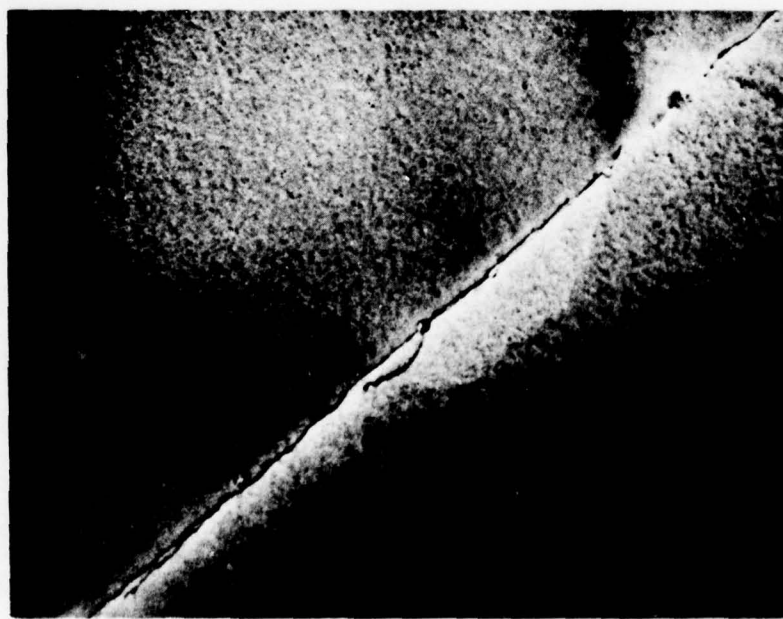
(a)



$2 \times 10^{18} \text{ P/cm}^3$

700°C Annealed CdTe: P;  $p_{\text{Cd}} = 2.4 \times 10^{-5} \text{ atm.}$

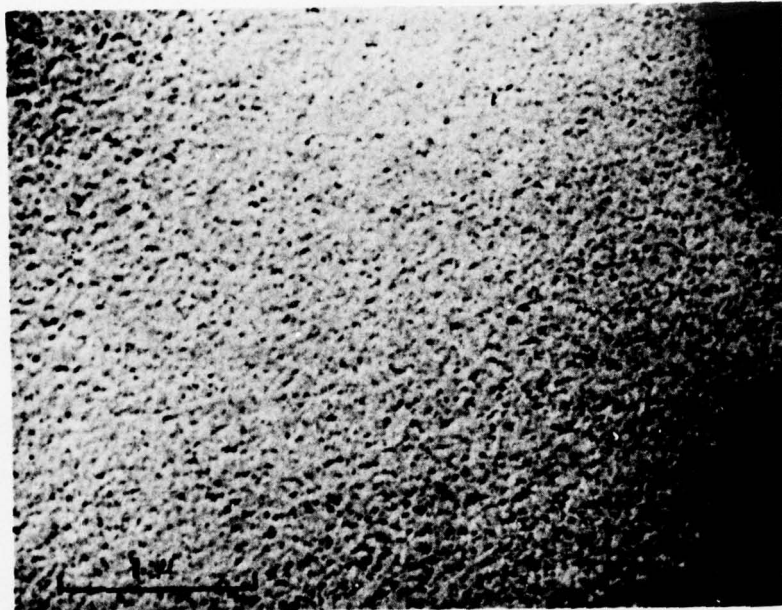
(b)



$6 \times 10^{16} \text{ P/cm}^3$

FIG. 3

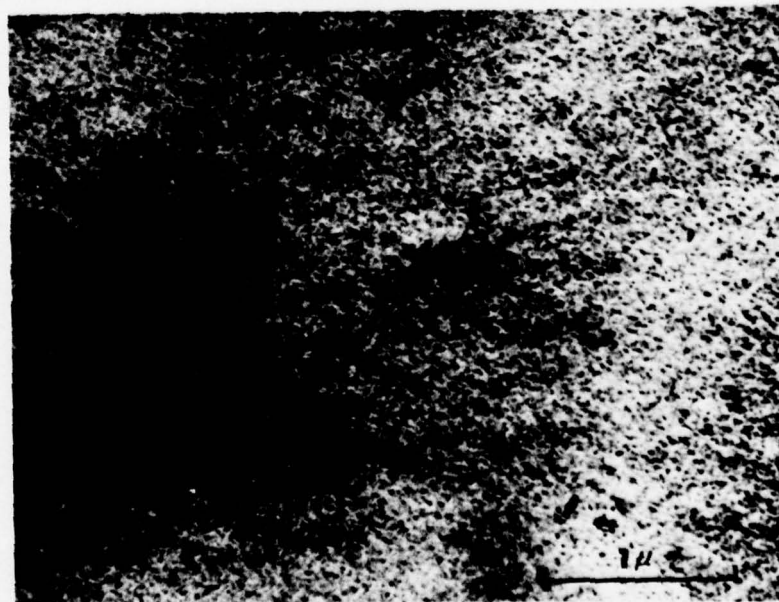
(a)



$6 \times 10^{16} \text{ P/cm}^3$

700°C Annealed CdTe:P;  $p_{\text{Cd}} = 1 \times 10^{-2} \text{ atm.}$

(b)



$2 \times 10^{17} \text{ P/cm}^3$

FIG. 4

Study of Defects in II-VI Compounds

F.A. Kröger, F.A. Selim and A. Ray

CdTe:P

The work on CdTe:P is completed. A defect model is proposed containing  $P_{Te}$  and  $P_i$  as the acceptors at high and medium  $p_{Cd}$ , respectively, and  $P_{Cd}$  as a triple donor at low  $p_{Cd}$ . Solubility data by Woodbury and Hall are explained assuming  $(P_i P_{Cd})^x$  as the major phosphorus species at low  $p_{Cd}$ , the acceptor species mentioned above as the major P species at high  $p_{Cd}$ . Local mode studies by Dutt and Spitzer indicate the presence of both  $P_{Cd}$  and  $(P_i P_{Cd})^x$  but not of  $P_i$ . Publication: F.A. Selim and F.A. Kröger "The Defect Structure of P-Doped CdTe", submitted to J. Electrochemical Society.

CdTe + Ge

Measurements on the carrier concentration and  $10.6\mu\text{m}$  absorption of CdTe +  $10^{17}\text{ Ge cm}^{-3}$  quenched after equilibration at  $700^\circ\text{C}$  in various cadmium pressures previously showed  $\alpha_{10.6} = 3 \times 10^{-2} \text{ cm}^{-1}$  at  $c_h = 10^{16} \text{ cm}^{-3}$  and  $\alpha_{10.6} = 3 \times 10^{-3} \text{ cm}^{-1}$  at  $10^{15} \text{ cm}^{-3} > c_h > 10^{13} \text{ cm}^{-3}$ . Repetition of these experiments led to values of  $\approx 4 \times 10^{-3} \text{ cm}^{-1}$  after annealing at medium  $p_{Cd}$ .

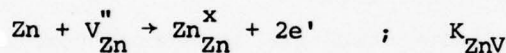
We have grown new ingots with  $10^{17}\text{ Ge cm}^{-3}$ ,  $10^{16}\text{ Ge cm}^{-3}$ , and  $(10^{17}\text{ Ge} + 10^{17}\text{ In})\text{cm}^{-3}$  and are ready to anneal these and measure  $10.6\mu\text{m}$  absorption.

ZnSe

Measurements of the high-temperature Hall effect and resistivity of ZnSe doped with 3 ppm Al, 30 ppm Al and 300 ppm Al, equilibrated with various partial pressures of zinc show an electron concentration

$c_e \propto p_{Zn}^{1/2} [Al]^{1/2}$  at medium  $p_{Zn}$ . The samples with 3 and 30 ppm Al show a constant electron concentration with  $c_e \approx c_{Al}$  at high  $p_{Zn}$ .

After cooling to room temperature, the samples annealed at 800°C at high and medium  $p_{Zn}$  show the same electron concentrations found at high temperature with a sharp cut-off at  $p_{Zn} = 3.15 \times 10^{-4}$  atm for the sample with 3 ppm Al and  $p_{Zn} = 8 \times 10^{-5}$  atm for the sample with 300 ppm Al. Below the cut-off the samples have a high resistivity. The cut-off is probably due to the trapping of electrons at  $V_{Zn}^{\prime}$ . The proportionality of  $c_e \propto p_{Zn}^{1/2} [Al]^{1/2}$  at low  $p_{Zn}$  is explained by a defect model in which the major charged defects are  $Al_{Zn}^{\bullet}, V_{Zn}^{\prime\prime}$  or  $Se_i^{\prime\prime}$ :



$$[e']^2 = K_{ZnV} p_{Zn} [V_{Zn}^{\prime\prime}] \approx 1/2 K_{Zn} V p_{Zn} [Al_{Zn}^{\bullet}]$$

The temperature dependence of the electron concentration at constant  $p_{Zn}$  and  $[Al]$ ,

$$[e'] \propto \exp + 0.5 \text{ eV}/kT$$

shows that  $1/2H_{Zn,V} = -0.5 \text{ eV}$  or  $H_{Zn,V} = -1 \text{ eV}$

A sample doped with 50 ppm As (an acceptor) annealed at 800, 900, 1000°C under various  $p_{Cd}$  shows still a negative Hall effect at high and medium  $p_{Zn}$  with  $c_e \propto p_{Zn}^{1/2}$  but now the temperature dependence is in the opposite direction:

$$[e'] \propto \exp -0.8 \text{ eV}/kT$$

indicating a positive energy of activation. This is to be expected for a defect model dominated by

$$[\text{As}'_{\text{Se}}] \approx 2[\text{V}^{\bullet\bullet}_{\text{Se}}] \quad \text{or} \quad 2[\text{Zn}^{\bullet\bullet}_i]$$

$$[e']^2 = K_{\text{Zn},V} p_{\text{Zn}} [\text{V}^{\bullet\bullet}_{\text{Zn}}] = K_{\text{Zn},V} p_{\text{Zn}} K_S [\text{V}^{\bullet\bullet}_{\text{Se}}]^{-1} = 2K_{\text{Zn},V} K_S p_{\text{Zn}} [\text{As}'_{\text{Se}}]^{-1}$$

or a similar expression with  $K_F$  instead of  $K_S$

Thus  $H_S$  (or  $H_F$ ) +  $H_{\text{Zn},V}$  = 1.6 eV or, with  $H_{\text{Zn},V} = -1$  eV,  $H_S$  (or  $H_F$ ) = 2.6 eV

The absolute value of  $[e']$  measured in the sample doped with As are similar to those reported by Smith for undoped ZnSe. On the other hand the activation energy found by Smith<sup>1)</sup>, 1.6 eV  $\pm$  0.2 eV is the same as the one found by us. Therefore it is likely that Smith's crystal was unintentionally doped with acceptors at a concentration not too different from the As concentration in our crystal.

#### ZnSe:Ga

Attempts to measure the high-temperature Hall effect on samples doped with 3 and 30 ppm Ga in equilibrium with atmospheres of known  $p_{\text{Zn}}$  were unsuccessful.

Crystals doped with 100 ppm Ga, quenched after annealing at 800°C at high  $p_{\text{Zn}}$  were n-type with a concentration of electrons  $<$  concentration of Ga. Crystals annealed at low  $p_{\text{Zn}}$  had a high resistance.

Robinson and Kun<sup>2)</sup> found p-type conductivity for ZnSe:Ga after annealing under  $p_{\text{Zn}}$  indicating acceptor behavior of Ga. On the other hand Tyagi and Arora<sup>3)</sup> report n-type behavior ( $2 \times 10^{16} \text{ e}' \text{ cm}^{-3}$ ) for ZnSe annealed

with Ga+Zn at 950-700°C. Yet acceptor behavior of Ga is indicated also in this case by the fact that ZnSe+Ga annealed in zinc vapor has a lower electron concentration than pure ZnSe under the same conditions<sup>4)</sup>. It is likely that Ga shows amphoteric behavior, acting completely or partly as an acceptor at high  $p_{Zn}$  but as a donor at medium and low  $p_{Zn}$ . Further work is needed to clarify the defect model.

References:

1. F.T.J. Smith, Solid State Commun. 7, 1757 (1969).
2. R.J. Robinson and Z.K. Kun, Appl. Phys. Letters 27, 74 (1975).
3. M.S. Tyagi and S.N. Arora, Phys. Stat. Solidi 32(a), 165 (1975).
4. M. Aven, D.T.F. Marple and B. Segall, J. Appl. Phys. 32, 2261 (1961).

## Absorption Studies of CdTe and ZnSe

W. G. Spitzer and B. V. Dutt

This section deals with absorption mechanisms in CdTe and ZnSe, particularly impurity-related absorption and free carrier absorption.

### A. Background and Summary of Our Previous Work.

Studies of infrared absorption of doped CdTe and ZnSe have been the subject of our previous progress reports. The dopants chosen were Al and P, as they are light in mass compared to the host atoms. This choice enables identification of the defects responsible for the observed absorption, since the free carrier absorption is reduced due to the prevalent self-compensation observed in II-VI compounds. Free carrier absorptions can be introduced by annealing in controlled partial pressures of the constituents. Throughout the investigations the primary long range goal has been to identify the various absorption mechanisms and their spectral range of influence. It is generally known that the various factors limiting the transparency of the II-VI compounds are multiphonon absorption, absorption due to precipitates or clusters of impurities or native defects, and inter- and intra-band carrier absorption involving electronic transitions. All these factors, except the multiphonon processes, are largely influenced by the conditions under which the crystals are grown and/or post-growth anneals. A substantial effort has been directed to preparing our own crystals and studying the influence of post-growth anneals on the contributions of the various absorption mechanisms. The following sections briefly summarize our work on CdTe:Al, ZnSe:Al, and CdTe:P previously reported in detail.

(1) CdTe:Al. It is usual to add donor elements In or Cl to CdTe to promote self-compensation. This results in a high resistivity material that is quite transparent in the infrared. Various defect models involving the presence of unassociated

$\text{In}_{\text{Cd}}^{\bullet}$ ,  $\text{V}_{\text{Cd}}^{\bullet\bullet}$ , associates  $(2\text{In}_{\text{Cd}}^{\bullet}\text{-}\text{V}_{\text{Cd}}^{\bullet})^x$ ,  $(\text{Cl}_{\text{Te}}^{\bullet}\text{-}\text{V}_{\text{Cd}}^{\bullet})^y$ ,  $(2\text{Cl}_{\text{Te}}^{\bullet}\text{-}\text{V}_{\text{Cd}}^{\bullet})^z$  have been proposed. These models were largely based on indirect evidence obtained from transport measurements. The infrared localized vibrational mode technique is a more direct way of identifying the defect species, although it is limited to elements considerably lighter than the host crystal atoms. Therefore, the choice for a donor is essentially restricted to the element Al. The electrical behavior of Al should be similar to In in CdTe. We therefore grew CdTe:Al crystals which were intentionally doped with an  $[\text{Al}] \approx 10^{19} \text{ cm}^{-3}$ . The introduction of counterdopants such as Cu, Ag and Au, usually by diffusion, was found to be useful for the identification of the different Al-related defect species. Full details of this work, giving possible defect assignments, has been reported elsewhere.<sup>1</sup> When CdTe:Al was annealed in Cd-rich conditions, free carrier absorption was observed. The absorption is nearly temperature independent, and shows  $\alpha(\nu) \sim \nu^{-3}$  and  $\nu^{-4}$  after appropriate anneals. The  $\nu^{-3}$  behavior was explained in terms of polar optical mode scattering and the  $\nu^{-4}$  behavior was accounted for in terms of ionized impurity scattering. There were two major concerns that were noted: the absence of temperature dependence in the  $\alpha \sim \nu^{-3}$  measurements and the better than expected results that the theory gave at the higher carrier densities  $\sim 10^{18} \text{ cm}^{-3}$ , where plasmon-phonon coupling is expected to cause the theory to be invalid.

(2) CdTe:P. This work was started primarily to understand the self-compensation mechanisms through the use of LVM techniques in acceptor-doped II-VI compounds. The material was grown in our laboratory by using the horizontal Bridgman method. Previous progress reports contain details of our absorption measurements on this system. The work is now complete and has been submitted for publication.<sup>(2)</sup> The major findings are:  
(a) there are two P defect centers, one  $\text{P}_{\text{Te}}$  or  $\text{P}_i$  center having  $T_d$  symmetry and the other a P-complex with axial symmetry;

(b) the  $P_{Te}$  or  $P_i$  is a shallow acceptor, while the P-complex appears to be a neutral center; (c) the shallow acceptors  $P_{Te}$  or  $P_i$  are present in unassociated form and native donors, such as Cd interstitials, account for the observed self-compensation.

(3) ZnSe:Al. The crystals used in this work were from Czochralski-grown ingots from Eagle-Picher Co. A set of ZnSe:Al was annealed in Zn-rich conditions and some free carrier absorption measurements were previously reported. The free carrier absorption shows  $\alpha(v) \sim v^{-3}$  behavior and is nearly temperature independent. These results are now analyzed and will be presented in a later section.

We also carried out LVM measurements on ZnSe:Al with Cu, Ag or Au. Infrared LVM bands attributed to pair defects of Al-Cu, Al-Ag or Al-Au were observed. These were very similar to the corresponding defects in CdTe. The results have been published elsewhere.<sup>(3)</sup>

#### B. Work Done During the Present Progress Report Period.

(1) CdTe:P. The work on this system has been completed and presented for publication.<sup>(2,4)</sup> Some of the findings were already mentioned in the above background and summary section. In order to better understand some of the unresolved details of the sources of defect-induced absorption in CdTe:P, we have initiated studies of the  $Zn_x Cd_{1-x} Te:P$  and  $Mg_x Cd_{1-x} Te:P$  binary alloy systems. The crystals were all grown using the horizontal Bridgman method. The absorption spectra are obtained at 80°K on the as-grown samples. The free carrier absorption is low and did not cause any problems of measuring the LVM bands from P-related defects. Preliminary indications are that the two systems behave differently with respect to the originally observed P defects. The results are being analyzed and will be reported later.

(2) ZnSe:Al. In continuation of our previous work, we have now carried out detailed calculations of free carrier absorption of ZnSe by using the theory for polar optical mode scattering.<sup>5</sup> The spectral dependence of the absorption, the nearly linear dependence on carrier density, the independence of the Al concentration and the magnitude of the absorption cross section are all in accord with this theory. However, as noted earlier, the free carrier absorption measurements showed nearly temperature independent absorption between 300°K and 80°K. This fact cannot be reconciled with the present theoretical model for polar optical mode scattering absorption. This behavior of annealed ZnSe:Al is very similar to that noticed earlier for CdTe:Al.<sup>1</sup> Full details of our work are in preparation for publication.<sup>5</sup>

References:

1. B. V. Dutt, M. Al-Delaimi and W. G. Spitzer, "Point Defects, Localized Vibrational Modes and Free-carrier Absorption of CdTe:Al," *J. Appl. Phys.* 47, 565 (1976).
2. B. V. Dutt and W. G. Spitzer, "A Localized Vibrational Mode Study of Infrared Absorption of CdTe:P," submitted for publication (JAP).
3. B. V. Dutt and W. G. Spitzer, "Localized Vibrational Modes of Al Paired with Cu, Ag, or Au in ZnSe," *J. Appl. Phys.* 47, 573 (1976).
4. B. V. Dutt and W. G. Spitzer, "Impurity Induced Absorption in P-doped CdTe," submitted for inclusion in the Proceedings of the Fifth Laser Window Conference, Las Vegas, Dec. (1975).
5. B. V. Dutt, O. K. Kim and W. G. Spitzer, "Free Carrier Absorption of n-type ZnSe:Al" (in preparation).

### High Power Infrared Laser Damage Studies

M. Bass

This part of the program is concerned with CO<sub>2</sub>, DF and HF pulsed laser induced damage studies. We have shown that the surface and bulk damage threshold of several materials at 10.6  $\mu\text{m}$  depends not only on such beam parameters as pulse duration and irradiation area, but also on the sequence of pulses used. These results are described in Ref. 1 (see Attachment A) and point up the necessity for re-examination of the conclusions drawn about damage mechanisms from measurements of relative damage thresholds.

Having obtained reliable performance from the infrared modulator, (see Fig. 1), we are starting to secure the data necessary for survival curve analyses of the 10.6  $\mu\text{m}$  damage mechanisms in IR window materials. This powerful diagnostic technique was described originally by Milam et al.<sup>2,3</sup> In order to obtain more accurate data recording, a computer controlled data acquisition system was requested for the current program. As a result of delays in contract negotiations, this system was not ordered until April of 1976 and is not expected to be available for use before mid-July. It appears, therefore, that the survival curve studies will be only partially completed by the end of the current project.

In this program, we have started the first pulsed laser damage studies in the 2-5  $\mu\text{m}$  region of the spectrum. This part of the project has been conducted jointly with the Naval Weapons Center (NWC) at China Lake, California. Our initial efforts were aimed at operating and characterizing the HF/DF TEA laser at NWC. We found that the laser's energy output was so irreproducible on a pulse to pulse basis that constant monitoring was required. The dependence of the pulse waveform on the wavelength of oscillation made it difficult to obtain reliable data and showed the need for single line operation. In addition, a believable measurement of the focal spot diameter has not yet been obtained

because the light burns the pinholes used to scan the beam. However, under these circumstances we have been able to study the relative damage thresholds of several materials of interest. Our results for this initial effort are listed in Table I with several other possibly related material properties. Table II lists the scattering data obtained for 2-5  $\mu\text{m}$  window materials in this work. From the fact that several samples have a poorly defined threshold in a 1 on 1 experiment, we can say that inclusion damage appears to be prevalent. It is also clear that current finishing techniques do not produce damage resistant surfaces. In fact, the differences between bulk and surface thresholds are in most cases greater than would be predicted on the basis of field enhancement at polishing imperfections.<sup>4</sup> If "vee" grooves were present all over the surface, field enhancement could explain the damage data but microscopy does not show a sufficient density of such grooves. The fact that field enhancement can not adequately explain the difference in damage thresholds may indicate that the surfaces are contaminated by absorptive polishing compounds or that as a result of polishing they are highly absorptive. Damage studies of etched surfaces and calorimetric measurements of surface and bulk absorption are planned.

To obtain more quantitative data, the laser is being more accurately characterized and, if possible, single line operation with damaging intensities will be obtained. Several other candidate materials will be studied and correlations sought between 2-5  $\mu\text{m}$  damage thresholds and other material properties.

We have attempted to secure the most up to date and promising materials for damage testing. We have obtained the most recent CVD grown ZnSe from Raytheon, RAP processed KCl and NaCl from Hughes Research Laboratories and pressed forged KCl from Honeywell. The latter was found to be recrystallized but will be studied while a new sample is prepared. Initial data on the new ZnSe was presented in Ref. 5. We are currently preparing this material using an etching procedure developed at Hughes and survival curve studies are in

progress. The RAP processed samples are being finished and a RAP processed KBr sample is being sent to us from the Naval Research Laboratories. We have arranged with the Hughes Research Lab to provide us with samples of improved 10.6  $\mu\text{m}$  AR coatings for damage resistance testing. These are expected to start arriving in May.

References:

1. M. Bass and K. M. Leung, IEEE J. Quantum Electron. QE-12, 82 (1976); also presented at the Fifth Laser Window Conference, Las Vegas, Nev., Dec. 1975.
2. D. Milam, R. A. Bradbury, R. H. Picard and M. Bass, "Statistical Technique for Detecting Inclusion Damage," 1973 High Power Laser Window Conference, Hyannis, Mass., Nov. 1973.
3. D. Milam, R. A. Bradbury, R. H. Picard and M. Bass, 1974 ASTM-NBS Laser Damage Conference, Boulder, Colo., May 1974.
4. N. Bloembergen, Appl. Opt. 12, 661 (1973).
5. K. M. Leung, M. Bass and A. J. G. Balvin-Villaverde, 1975 ASTM-NBS Laser Damage Conference, Boulder, Colo., July 1975.

Table I. Relative Damage Thresholds Using "Al-line" DF "TEA" Laser and Other Properties

	$I_{SF}$ GW/cm <sup>2</sup>	$I_B$ GW/cm <sup>2</sup>	Bulk Threshold Normalized to the Value for NaCl	Index of Refraction $n$	Total Absorptivity (bulk & surface)	Knoop Hardness $\beta$ (cm <sup>-1</sup> )	Melting Point °C
Alkaline Earth-halides							
MgF <sub>2</sub>	16.5 <sup>†</sup>	18.5 <sup>†</sup>	1.19	1.355	$4.8 \times 10^{-4}$	415	1255
CaF <sub>2</sub>	5.9	25.5	1.65	1.41	$\sim 3.5 \times 10^{-4}$	120	1395
SrF <sub>2</sub>	7.7	28.5	1.84	1.41	$\sim 6 \times 10^{-4}$	130	1450
BaF <sub>2</sub>	9.75	27.5	1.77	1.457	$\sim 18.5 \times 10^{-4}$	65	1355
Alkali Halides							
LiF	9.0 <sup>†</sup>	20.0 <sup>†</sup>	1.29	1.353	$25.5 \times 10^{-4}$	102	844
NaF	10.3	>30.0	>1.94	1.31	$5.2 \times 10^{-4}$	60	1012
NaCl	-----	15.5	1	1.52	$4.2 \times 10^{-4}$	18	801
Al <sub>2</sub> O <sub>3</sub>	-----	25.0	1.61	1.68	$4 \times 10^{-2}$	~1700	2040

<sup>†</sup>These are median values of widely separated minimum fluxes for damage and maximum for no damage. Suggests that these media are inclusion damage limited.

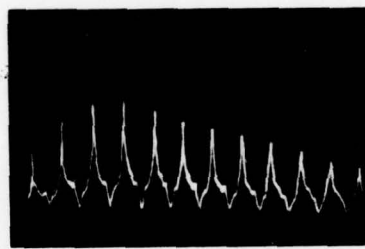
Table II. Scattering\* in 2-5 $\mu$ m Window Materials

Material	$\lambda(\mu\text{m}) = 0.4762$		$\lambda(\mu\text{m}) = 0.6471$		$\lambda(\mu\text{m}) = 1.15$		$\lambda(\mu\text{m}) = 3.39$	
	Forward		Backward		Forward		Backward	
	Forward	Backward	Forward	Backward	Forward	Backward	Forward	Backward
MgF <sub>2</sub>	2.23 × 10 <sup>-3</sup>	1.62 × 10 <sup>-3</sup>	1.68 × 10 <sup>-3</sup>	9.00 × 10 <sup>-3</sup>	0.554 × 10 <sup>-3</sup>	0.282 × 10 <sup>-3</sup>	0.404 × 10 <sup>-3</sup>	0.0307 × 10 <sup>-3</sup>
CaF <sub>2</sub>	3.64	4.54	2.15	2.36	0.960	0.541	0.532	0.532
BaF <sub>2</sub>	2.43		1.41	1.47	0.455		0.157	0.0558
SrF <sub>2</sub>	1.98	2.68	1.16	1.39	0.404	0.318	0.179	0.0495
NaF	14.1	13.8	7.64	8.53	1.75	2.30	0.184	0.210
LiF	4.14		2.29	3.03	0.564		0.0973	0.0700

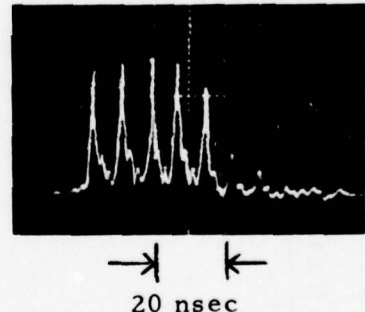
\*Scattering is the fraction of the light scattered into the forward or backward  $2\pi$  radians with respect to the total quantity of light transmitted through the sample.

Figure 1

CO<sub>2</sub> TEA laser  
waveform before  
modulator



Waveform trans-  
mitted through  
switched modulator



(Photos retouched for clarity when printed.)

## ATTACHEMENT A

TABLE I  
SUMMARY OF EXPERIMENTAL PARAMETERS

Laser	$\text{CO}_2$ TEA
Wavelength	10.6 $\mu\text{m}$
Waveform	9.7 nsec gain-switched pulse with self mode-locked spikes $\leq 2.5$ nsec duration and 8 nsec interpulse spacing
Transverse mode	$\text{TEM}_{60}$
Attenuation	ZnSe beam splitter and two Brewster angle stacked plate polarizers
Focusing lens	Ge, 3.8 cm focal length, aberration free
Focal spot diameter	107 $\mu\text{m}$ to $1/e^2$ in intensity
Detection system	Photon drag detectors and Tektronix 7844 Oscilloscope. Riserate = 2.5 nsec

The Dependence of the Pulsed 10.6- $\mu\text{m}$  Laser Damage Threshold on the Manner in Which a Sample is Irradiated

M. BASS AND K. M. LEUNG

**Abstract-** The threshold for pulsed 10.6- $\mu\text{m}$  laser-induced surface and bulk damage in transparent materials has been shown to depend on the manner in which the samples are irradiated. When a site is irradiated several times, starting at a very low intensity and increasing the flux a few percent on successive shots until damage occurs, the threshold is often higher than if each site were irradiated only once. In addition, it has been shown that the damage threshold also depends on the sample tested and so the use of relative damage-threshold measurements to identify the damage mechanism should be reexamined.

Thresholds for pulsed laser damage to transparent media have been determined in a variety of experiments. The importance of the beam's spatial mode and the pulse's temporal waveform have been discussed [1]. There has also been extensive discussion of the relation between the size of the irradiated volume and the measured threshold [2]. In this correspondence, we point out the importance of the number of times a site is irradiated in determining the reported damage threshold at 10.6  $\mu\text{m}$  and how this fact affects comparisons between materials.

We have reported experiments in which each site was irradiated only once and the intensity was increased at each successive site until damage was produced with some degree of consistency (i.e., 50 percent of the sites are damaged) [3]. Allen *et al.* reported damage thresholds obtained when each site was irradiated several times starting at a very low intensity and increasing the flux a few percent on successive shots until damage occurred [4]. Since our one shot on one site (1-on-1) and their several shots on one site (*N*-on-1) experiments gave different results for the same materials, we have undertaken a direct comparison of these procedures on the same samples.

Our experiment is described in detail in [3] and is summarized in Table I. The results of our 1-on-1 and *N*-on-1 comparison are given in Table II. Clearly, when the diameter of the irradiated region is  $\sim 100$   $\mu\text{m}$ , the 10.6- $\mu\text{m}$  laser damage threshold of ZnSe is independent of the manner of irradiation. KCl and NaCl, on the other hand, have higher damage thresholds when measured in an *N*-on-1 experiment than in a 1-on-1 experiment. This increased threshold is observed for  $\sim 50$  percent of the sites studied in both surface and bulk damage ex-

periments. No dependence on interpulse interval was found for a range from 5 s to  $> 1$  min.

As in [3], we also monitored the transmitted pulse waveform distortion during these experiments. We found that in an *N*-on-1 experiment no distortion could be detected during any pulse prior to the one which produced a spark and left residual damage in the sample. The distortion of the last pulse was, in all respects, similar to that seen in a 1-on-1 damage measurement.

The increase in surface damage threshold in an *N*-on-1 experiment might be due to either a cleaning of the surface by the laser at low intensities [5] or a smoothing out of the sharp edges of polishing scratches by some form of "laser polishing." If sharp edges are removed and "vee"-like scratches become more nearly cylindrical, Bloembergen [6] would predict a ratio of damage intensities for *N*-on-1 to 1-on-1 of

$$R = \frac{(\epsilon + 1)^2}{4}$$

where  $\epsilon = n^2$  is the optical frequency dielectric constant, and  $R$  is the ratio of the square of Bloembergen's field-enhancement factors for "vee" grooves to that for cylindrical grooves. Thus, for NaCl where  $n = 1.49$ , we should have  $R_{\text{NaCl}} = 2.59$  and for KCl where  $n = 1.46$  we should have  $R_{\text{KCl}} = 2.45$ . From Table II we see that the experimental ratios are 3.06/3.33 and 2.36, respectively. In other words, the change in the surface damage threshold between the *N*-on-1 and 1-on-1 experiments does not disagree with the "laser-polishing" explanation. The fact that the surface damage threshold of ZnSe is independent of the type of experiment may be due to the fact that the damage mechanism in this material is absorption by particulate inclusions [3]. This mechanism is not sensitive to local field enhancement.

The foregoing model might explain the results for surface damage, but does not suffice when we consider the results for bulk damage. The increased damage flux in an *N*-on-1 experiment for bulk damage is both unexpected and troublesome. Consider, for example, the fact that the ranking of the two NaCl samples reverses when one goes from a 1-on-1 threshold to an *N*-on-1 value. Consider, in addition, comparing KCl to NaCl. For each type of experiment one gets a different relative damage threshold. The fact that the relative damage threshold also depends on which samples are compared suggests that the use of such comparisons to identify the damage mechanisms [7] be reexamined.

In studying the statistics of laser damage, at 1.06 and 0.69  $\mu\text{m}$  the site was irradiated several times with pulses of fixed intensity [8]. The irradiation continued until either damage occurred or until some predetermined number of pulses had

Manuscript received September 11, 1975. This work was supported by the Defense Advanced Research Projects Agency, and was monitored by the Air Force Cambridge Research Laboratory.

The authors are with the Center for Laser Studies, University of Southern California, Los Angeles, CA 90007.

TABLE II  
COMPARISON OF N-ON-1 AND 1-ON-1 LASER DAMAGE THRESHOLDS

Material	10.6 $\mu\text{m}$ Damage Threshold <sup>a</sup> in $\text{mJ}/\text{cm}^2$									
	N-1		KCl		NaCl					
Supplier's Designation	Rutherford Elec. Lab.	Harshaw Economat Grade	HR1 RAP Grown		Harshaw Economat Grade	Harshaw Spectrophotometer Grade				
	Surface	Bulk	Surface	Bulk	Surface	Bulk	Surface	Bulk		
Type of Experiment	N-on-1	0.35	0.41	1.3	2.0	2.6	4.9	7.1	2.8	14.0
	1-on-1	0.35	0.46	1.56	0.65	1.5	1.6	6.1	0.84	3.9
$\frac{\text{N-on-1}}{\text{1-on-1}}$		1.0	1.0	2.36	3.07	2	1.73	3.06	3.33	3.58

<sup>a</sup>Defined as that intensity which damages 50 percent of the sites.

been tried. At any particular intensity level the distribution of the number of pulses required to produce damage was given by the binomial distribution [8], [9]. This is a characteristic of a process having a constant probability of occurrence on each trial. If low-level irradiation caused an increase in the damage threshold of the materials studied at 1.06 and 0.69  $\mu\text{m}$ , then the damage probability would not have been constant from pulse to pulse. The probability for damage would have decreased on each successive pulse so that if damage did not occur on the first pulse it would very likely not have occurred at all. The process would have appeared thresholdlike instead of statistical. We feel, therefore, that the increased threshold in an N-on-1 experiment at 10.6  $\mu\text{m}$  does not conflict with the statistical properties of 1.06- and 0.69- $\mu\text{m}$  laser damage. In fact, the statistics observed at the shorter wavelengths suggest that there would be no increase in threshold in an N-on-1 experiment performed with either an Nd or a ruby laser.

The measured 10.6- $\mu\text{m}$  laser damage threshold for both bulk and surface damage in some materials has been shown to depend on the procedure used. This study has also shown that the relative ranking of materials according to their damage thresholds depends on which samples are compared and on the experimental procedure. As a result, the use of such rankings to identify the laser damage mechanism should be reexamined.

Note Added in Proof: No increase in bulk damage threshold for the sample of NaCl (Harshaw Spectrophotometer Grade) was observed in an N-on-1 experiment as compared to a 1-on-1 experiment performed with a ruby laser.

#### ACKNOWLEDGMENT

The authors wish to thank C. Tang and M. Chang for their assistance in this work. They also wish to thank V. Wang, who participated in the initial experiments.

#### REFERENCES

- [1] M. Bass, "Laser induced damage to nonlinear crystalline materials," NBS Special Publ. 341, pp. 90-96, Dec. 1970.
- [2] L. G. DeShazer, B. E. Newnam, and K. M. Leung, "The role of coating defects in laser-induced damage to thin films," NBS Special Publ. 387, pp. 114-123, Dec. 1973.
- [3] K. M. Leung, M. Bass, and A. G. J. Balbin-Villaverde, "Damage to 10.6  $\mu\text{m}$  window materials due to CO<sub>2</sub> TEA laser pulses," presented at the 1975 Laser Damage Symp., Boulder, CO, July 1975, and to appear in the proceedings of that meeting.
- [4] S. D. Allen, M. Braunstein, C. Giuliano, and V. Wang, "Pulsed CO<sub>2</sub> laser damage studies of RAP grown KCl," NBS Special Publ. 414,

pp. 66-75, Dec. 1974.

- [5] T. L. Barber, "Degradation of laser optical surfaces," ECOM Rep. 5237, Mar. 1969.
- [6] N. Bloembergen, "The role of cracks, pores and absorbing inclusions on laser induced damage threshold at surfaces of transparent dielectrics," *Appl. Opt.*, vol. 12, pp. 661-664, Apr. 1973.
- [7] E. Yablonovitch, "Optical dielectric strength of alkali-halide crystals obtained by laser induced breakdown," *Appl. Phys. Lett.*, vol. 19, pp. 495-497, Dec. 1971.
- [8] M. Bass and H. H. Barrett, "Avalanche breakdown and the probabilistic nature of laser-induced damage," *IEEE J. Quantum Electron.*, vol. QE-8, pp. 338-343, Mar. 1972.
- [9] M. Bass and D. W. Fradin, "Surface and bulk laser damage statistics and the identification of intrinsic breakdown processes," *IEEE J. Quantum Electron.*, vol. QE-9, pp. 890-896, Sept. 1973.

Surface Absorption Studies with Acoustic Probe Techniques  
J. H. Parks and D. A. Rockwell

This final report discusses the completion and accomplishments of an experimental program which applied acoustic surface wave technology to the problem of measuring the weak radiative absorption occurring within a thin layer at the surface of a dielectric solid. Details of these studies including analysis and application to KCl samples are presented in the following pages in the form of two technical papers presently accepted for publication in the Journal of Applied Physics.

As a general overview of the program, the surface acoustic wave techniques were found to be an extremely sensitive tool which could be used to unravel the surface and bulk absorption of  $10.6\mu$  radiation in prepared KCl materials. It was observed that surface absorption as small as  $\sigma \sim 10^{-4}$  could be directly measured in the presence of rather large bulk absorption,  $\beta_B \sim 10^{-3} \text{ cm}^{-1}$ . A theory was derived to extract these radiative parameters from experimental data and in fact could fit the data over a wide range of experimental conditions. The experimental sensitivity, coupled with these analytical methods, suggest the capability of extending measurements of the surface absorption to  $\sigma \leq 10^{-5}$ . Experimental techniques were developed which allowed the surface waves to be fluid coupled to an arbitrary material under study. These techniques are straightforward and should provide the flexibility to apply the measurement technique to a wider class of materials. It should be noted, however, that polycrystalline materials for which the average grain size is comparable to the acoustic wavelength will introduce significant acoustic wave scattering. In this regard lower acoustic frequencies, for which the wavelength is comparable to  $50-100\mu\text{m}$ , have been observed to propagate on polycrystalline KCl. The extension of similar measurements to ZnSe appears a realistic possibility.

To summarize, the principal accomplishments of this program

include:

1. Application of surface acoustic wave technology to the measurement of weak surface absorption.
2. Derivation of a theory which was shown to extract radiative absorption parameters directly from experimental data.
3. Development of techniques to couple surface waves to arbitrary materials which in itself broadens the materials applicability of the measurement technique.

This technology is presently being transferred to the China Lake Naval Weapons Center, where, under the guidance of Dr. H. Bennett and Dr. D. White, it can possibly be put to expanded use.

STUDIES OF RADIATIVE ABSORPTION AT KCl SURFACES  
USING ACOUSTIC TECHNIQUES\*

D. A. Rockwell<sup>†</sup> and J. H. Parks<sup>‡</sup>

Departments of Physics and Electrical Engineering  
University of Southern California  
Los Angeles, California 90007

## ABSTRACT

The application of an acoustic technique to measure surface radiative absorption in highly transparent materials is presented. Dispersive phase changes in acoustic surface wave propagation are induced by the absorption of 10.6  $\mu\text{m}$  pulsed laser radiation on KCl surfaces. Analysis based upon an absorbing surface layer model provides a  $\pm 15\%$  determination of both the total surface absorption  $\sigma = 4.5 \times 10^{-4}$  and a bulk absorption coefficient  $\beta_B = 2 \times 10^{-3} \text{ cm}^{-1}$  for a mechanically polished/chemically etched surface. After mechanical repolishing, this sample yields  $\sigma = 11.3 \times 10^{-4}$ . The sensitivity of this technique indicates the possibility of measuring a surface absorption as small as  $\sigma \lesssim 10^{-5}$  and also obtaining details of the radiative absorption depth distribution.

PACS numbers: 78.50. - w, 81.80. + x

The weak radiative absorption occurring in laser window materials represents a practical problem limiting the application of high power lasers. Crystal growth procedures have developed the capability of growing highly pure materials with bulk absorption coefficients approaching intrinsic levels. As a result, major research efforts have been directed toward studying the residual surface absorption occurring within 1-10  $\mu\text{m}$  of the crystal surface. We present results<sup>1</sup> of a new technique to measure absorption of  $\text{CO}_2$  laser radiation on both mechanically and chemically polished KCl samples. These results indicate (i) high sensitivity to surface effects, (ii) the ability to separate surface and bulk absorption with measurements on a single sample, and (iii) the possibility of determining the detailed depth dependence of the absorptive properties.

The theory of acoustic surface wave detection of radiative absorption has been well established in quantitative studies on quartz<sup>2,3</sup> and lithium niobate.<sup>3</sup> The fundamental idea is that the temperature change induced in the material by the radiative absorption results in a change in the velocity of a continuous acoustic surface wave propagating through the absorbing region. For a fixed acoustic path length  $2L$  along the x-axis, the velocity change  $\Delta v_s$  manifests itself as a phase change given by<sup>3</sup>

$$\Delta\phi(t) = -\frac{4\pi\nu}{v_{so}} f_B \int_0^L \left[ \frac{\Delta v_s(x, t)}{v_{so}} \right] \lambda_s dx \quad (1)$$

where  $\nu$  is the frequency and  $v_{so}$  is the unperturbed velocity of the surface

wave. The subscript  $\lambda_s$  in the integrand indicates that, in general, the velocity change will depend on the acoustic wavelength  $\lambda_s$ . This velocity dispersion arises from propagation through the thermally-induced spatial inhomogeneity within the acoustic penetration depth  $\sim \lambda_s$ . The factor  $f_B$  results from an averaging over the transverse variation of both the acoustic wave amplitude and the temperature distribution. The phase change contribution due to constrained thermal expansion of the path length is generally  $\lesssim 1\%$  of  $\Delta\phi$  and has been omitted from Eq. (1). Nonlinear effects, such as the velocity change induced by thermoelastic stress are also neglected. Further description of the induced phase change follows two logical steps: (i) relate the temperature change to the absorptive properties of the material, and (ii) relate the acoustic velocity change to the temperature change.

In highly transparent materials the absorption coefficient  $\beta$  within 1-10  $\mu\text{m}$  of the surface can be significantly greater than that in the bulk. The extent of this surface absorption depends on surface preparation procedures, immediate environmental impurity adsorption, and perhaps the effect of surface dislocations induced during sample preparation. The simplest model that embodies these effects is an absorption layer model in which an absorbing surface region with  $\beta = \beta_s$  extends a distance  $d$  into the material, at which depth a transition to the bulk value  $\beta = \beta_B$  occurs. For example, in KCl at the 10.6  $\mu\text{m}$  laser wavelength, one might expect  $\beta_s \sim 10 \text{ cm}^{-1}$ ,  $d \sim 1 \mu\text{m}$ , and  $\beta_B \lesssim 10^{-3} \text{ cm}^{-1}$ . This set of surface parameters results in a total surface absorption

$\sigma_s = \beta_s d = 10^{-3}$ , which is typical for mechanically polished surfaces.

This absorption layer model is used to calculate the temperature change  $\Delta T(r, z, t)$  induced by radiative absorption. We consider a laser pulse of temporal width  $\tau_p$ , gaussian profile of width (HWHM)  $\alpha$  which propagates along the  $z$ -axis and is absorbed by the material. For pulsed widths considered in this work, the temperature variation in  $z$ , characterized by the depth dependence of  $\beta(z)$ , is much greater than radial variation characterized by the gaussian width  $\alpha$ . Radial diffusion is then negligible.

Consequently, the radial temperature profile is identical to the gaussian laser pulse, and the temperature  $\Delta T$  is found by solving a one-dimensional heat equation. (Rigorous solutions to the three dimensional heat equation justify this approximation.) The material is considered an infinite slab of thickness  $b$ , and all surface heat losses are neglected. The solution is most conveniently written in series form  $\Delta T(z, t) = \sum T_n(t; \beta_s, d, \beta_B) \cos k_n z$  where  $k_n = n\pi/b$ .

The dispersive velocity change  $[\Delta v_s / v_{s0}]_{\lambda_s}$  follows from a perturbative treatment<sup>4</sup> of the acoustic wave equation in which the elastic

coefficients exhibit spatial variation through their weak ( $\sim 10^{-4}/^{\circ}\text{K}$ )<sup>5</sup> temperature dependence.<sup>5</sup> We assume that thermal diffusion has extended the subsurface temperature distribution to a depth  $\gtrsim \lambda_s$  for which a volume perturbation theory is appropriate. Although the details of this calculation<sup>6</sup> are not essential to the present discussion, it is instructive to describe the functional form of the solution:

$$\left[ \frac{\Delta v_s(x, t)}{v_{so}} \right]_{\lambda_s} = \sum_{n=0}^{\infty} T_n(t; \beta_s, d, \beta_B) A(k_n \lambda_s) e^{-\left(\frac{x}{\lambda_s}\right)^2 \ln 2} \quad (2)$$

The function A approaches a constant for small values of its argument; its physical significance is that it introduces dispersion for terms such that  $k_n \lambda_s \gtrsim 1$ . Experimental measurements of this dispersion are useful in determining the absorption parameters since each  $\lambda_s$  provides a different weighted sum of the  $T_n$ . The coefficients  $T_n$  determine whether  $\Delta v_s / v_{so}$  is sensitive to  $\beta_s$  and d individually, or simply their product  $\sigma = \beta_s d$ , as follows. Detailed information on the spatial variation of  $\beta(z)$  is contained only in the coefficients with large n. For times  $\lesssim 10 \mu\text{sec}$ , Eq.(2) has significant contributions from such terms, and phase change measurements will determine d and  $\beta_s$  independently. For times  $\gtrsim 100 \mu\text{sec}$ , however, most of the high-n terms have decayed, and consequently the acoustic phase change is only sensitive to  $\sigma$ .

Experimental phase change measurements on KCl have been

obtained using the apparatus shown in Fig. 1. The signal from a stabilized VHF generator, amplified to  $\sim$  1 watt, launches surface waves on a quartz transducer crystal using interdigital transducers. The surface wave is fluid-coupled<sup>7</sup> onto the KCl sample, interacts with the radiatively induced temperature distribution, and is then fluid-coupled back to the transducer crystal. The reliability of this fluid-coupling process was previously shown in Ref. 7 and is reaffirmed by the present results. The transmitted signal enters the right channel of the double balanced mixer. The left channel receives a reference signal from the generator. The variable delay line is adjusted such that a transient phase change of the transmitted signal by an amount  $\Delta\varphi(t)$  yields a mixer output signal  $V_x = V_o \sin \Delta\varphi(t)$ , where  $V_o$  is typically 350 mV. The peak value of the phase change is measured at the time  $\tau_p$ , the end of the laser pulse. These peak values are detected and held by a peak detector, and averaged by a boxcar integrator. The pulse repetition rate is chosen to maintain the same average laser power for measurements at each pulselength  $\tau_p$ .

A CO<sub>2</sub> laser pulse of  $\sim$  65 watts is focused through a hole in the transducer crystal and is incident on a Harshaw KCl sample. Acoustic frequencies of 124.5, 62.1, and 28.0 MHz were used for which  $\lambda_s = 14.1, 28.2$  and  $62.5 \mu\text{m}$  respectively. Using a focused laser beam of width  $a = 0.2 \text{ mm}$ , the measured<sup>3</sup> values of  $f_B$  are .21, .25, and .185 at these three frequencies, respectively. Figure 2 shows representative oscilloscope traces of  $\Delta\varphi(t)$  for two pulselengths at 124.5 MHz. The 100 msec peak

phase change in Fig. 2a is 60 mrad corresponding to  $\Delta v_s / v_{so} = -2.2 \times 10^{-5}$  per watt for  $v_{so} = 1.753 \times 10^5$  cm/sec. The peak phase change of 2.1 mrad in Fig. 2b was obtained for a 0.5 msec 35mj laser pulse, and is about ten times greater than the measured rms noise of  $\sim 0.2$  mrad. This establishes the sensitivity of the acoustic technique and indicates the ability to study lower absorption coefficients and, if necessary, shorter pulsedwidths than are presented here. Experimental uncertainties arise from absolute uncertainties in the measurement of the following quantities:  $\sim \pm 5\%$  each in the laser power, the value of  $V_0$ , and possibly the fluid coupling scheme, and  $\sim \pm 10\%$  in the experimental determination<sup>3</sup> of  $f_B$ . These lead to an overall absolute uncertainty in these measurements of  $\sim \pm 15\%$ .

The data set taken on a sample surface which was both mechanically polished and chemically etched<sup>8</sup> is shown in Fig. 3a (referred to as chemical polish). The curves representing the theory are discussed below. Following these measurements, the same KCl sample was repolished mechanically in our laboratory using standard techniques, and a second set of measurements were taken. These mechanical polish results, shown in Fig. 3b, represent the two lower acoustic frequencies; in this case  $f_B$  is .33 and .25 for 62.1 and 28.0MHz, respectively. Comparison of the data in Figs. 3a and 3b indicates that the chemical etch reduces the surface absorption

by a factor of  $\sim 3$ . Similar results have been observed<sup>9</sup> in calorimetric measurements.

A least squares computer program varied the two parameters of the absorption model,  $\sigma = \beta_s d$  and  $\beta_B$ , to obtain the optimum fit of Eqs. (1) and (2) to the data. As is clear from Fig. 3, the theory represents an adequate description of the data except for the shorter times and lower frequencies. It is believed this short time discrepancy arises from a breakdown of the volume perturbation calculation of  $\Delta v_s / v_{s0}$  when the temperature depth dependence becomes comparable to the acoustic penetration depth which is  $\sim 2.2 \lambda_s$  for KCl. A separate fit, made to the 124.5 MHz data alone, is represented by the curve plotted in Fig. 3a. Because of the shorter penetration depth the theory is adequate at that frequency even for the shortest times. The data for both lower frequencies in Fig. 3a were fit simultaneously using pulsed widths  $\tau_p \geq 10$  msec. The average value of  $\sigma$  based on these two independent fits to the chemical polish data is  $\sigma = (4.5 \pm 5) \times 10^{-4}$  with  $\beta_B = 2 \times 10^{-3} \text{ cm}^{-1}$ . A simultaneous fit was also done for the data shown in Fig. 3b using the same pulsed widths, yielding  $\sigma = 11.3 \times 10^{-4}$  and  $\beta_B = 2 \times 10^{-3} \text{ cm}^{-1}$  for the mechanical polish data. These results for  $\sigma$  and  $\beta_B$  are consistent with calorimetric measurements<sup>10</sup> on these and similar samples.

Figure 4 shows the reduced phase change  $\Delta\varphi_R = \Delta\varphi / (\nu f_B)$  versus laser pulsed width  $\tau_p$  on the chemically polished surface. The reduced phase change is convenient in discussing dispersion since  $\Delta\varphi_R$  eliminates the trivial linear frequency dependence in Eq. (1) and also the uninteresting

effects arising from different acoustic profiles at each frequency. The divergence of the data for shorter times, when the subsurface temperature gradient  $\partial\Delta T/\partial z$  becomes comparable to  $\Delta T/\lambda_s$ , indicates the presence of a surface absorption layer even after significant material ( $\sim 10 \mu\text{m}$ ) was removed during the etching process. Such a temperature gradient could only arise from a rapid depth variation of  $\beta(z)$  on the scale of several microns. The importance of this figure is to establish the observation of dispersion well outside the experimental uncertainty even though the present theory is insufficient to describe data for longer wavelengths and shorter times.

The present results indicate the utility and sensitivity of this acoustic technique. Since the absorption of a 70 watt, 100 msec laser pulse on a surface with  $\sigma \sim 5 \times 10^{-4}$  induced a phase change of  $\Delta\varphi = 60 \text{ mrad}$  at 124.5 MHz, a readily measurable phase change of 1 mrad would result from a surface with  $\sigma \sim 10^{-5}$ . Dispersive measurements requiring data at lower frequencies are less sensitive and have a lower limit of  $\sigma \sim 10^{-4}$  based on the 28 MHz results. This limit is comparable to the lowest surface absorption measured on chemically polished samples.<sup>11</sup> Both limits could be further reduced by operating at higher laser power. In order to measure  $\beta_s$  and  $d$  independently, it is necessary to use pulse-widths  $\tau_p \lesssim 10 \mu\text{sec}$ . Present TEA lasers ( $\text{CO}_2$ , HF/DF) provide short pulses with sufficient energy for such measurements. The breakdown of the present theory for short times does not represent a practical limitation of this technique since theories presently exist<sup>4</sup> which describe surface

wave propagation in layered media. Such a theory could be used, for example, in a study of radiative absorption in films of thickness  $\lesssim 1 \mu\text{m}$  if laser pulsedwidths  $\lesssim 1 \mu\text{sec}$  are used to reduce the effect of thermal diffusion. The sensitivity of this technique suggests immediate application to several important measurements: (i) Details of  $\beta(z)$  near surfaces, (ii) Impurity diffusion into alkali-halide surfaces, and (iii) Absorption in thin dielectric or conducting films.

The authors wish to thank S. Allen and A. Timber of Hughes Research Laboratories for the KCl samples and their preparation. They also thank D. White and R. King of China Lake NWC for transducer fabrication, and D. Smith for his invaluable assistance in writing the computer programs.

## REFERENCES

\* Research supported by the Advanced Research Projects Agency.

† Present address: Laser Division, Hughes Aircraft Co., Culver City, California, 90230.

‡ Present address: Avco Everett Research Laboratory, Inc., Everett, Massachusetts 02149.

1. Preliminary results of these studies are presented in:  
D. A. Rockwell, T. S. Colbert, and J. H. Parks, in Proceedings of the International Conference on Optical Properties of Highly Transparent Solids, edited by S. S. Mitra and B. Bendow (Plenum, New York, 1975), p. 493.
2. J. H. Parks, D. A. Rockwell, T. S. Colbert, K. M. Lakin, and D. Mih, Appl. Phys. Lett. 25, 537 (1974).
3. D. A. Rockwell and J. H. Parks, to be published in J. Appl. Phys., manuscript No. 192R.
4. B. A. Auld, Acoustic Fields and Waves in Solids, (Wiley, New York, 1973), Vol. II, p. 271.
5. A compilation of these values for many materials is given in:  
Landolt-Börnstein, Numerical Data and Functional Relationships in Science and Technology, Vol. I, Elastic, Piezoelectric, Piezooptic and Electrooptic Constants of Crystals, K. H. Hellwege, editor in chief (Springer-Verlag, New York, 1966).
6. J. H. Parks and D. A. Rockwell, unpublished.
7. D. A. Rockwell and J. H. Parks, to be published in J. Appl. Phys., manuscript No. R9484.
8. These polishing methods are described in W. S. Ewing, Air Force Cambridge Research Laboratories Rpt. No. AFCRL-TR-74-0134 (AFCRL, Bedford, Mass. 1974).
9. H. F. Lipson, private communication, also Proceedings of the Fifth Conference on Infrared Laser Window Materials, to be published by Air Force Cambridge Research Lab., Bedford, Mass. See paper by H. Lipson and P. Ligor.
10. S. Allen, (private communication).
11. T. F. Deutsch, Appl. Phys. Lett. 25, 109 (1974).

### FIGURE CAPTIONS

Fig. 1      Experimental apparatus for studying radiative absorption at KCl surfaces using acoustic techniques.

Fig. 2      Oscilloscope traces of the mixer output showing the transient phase change induced on chemically polished KCl by 10.6  $\mu\text{m}$ , 70 watt laser pulses. (a) 4 mv/div, 20 msec/div,  $\tau_p = 100$  msec; (b) 0.4 mv/div, 2 msec/div,  $\tau_p = 0.5$  msec. The acoustic frequency is 124.5 MHz.

Fig. 3      Phase change data versus laser pulsedwidth at various frequencies for (a) chemical polish and (b) mechanical polish KCl surfaces. Bars indicate  $\pm 15\%$  experimental uncertainty. Solid curves are theoretical fits to the data.

Fig. 4      Phase change dispersion versus laser pulsedwidth is indicated by the increasing divergence of  $\Delta\varphi_R$  as  $\tau_p$  decreases. These data were taken on a chemically polished surface; experimental uncertainty is  $\pm 15\%$ . Dashed curves are shown as guides to the eye.

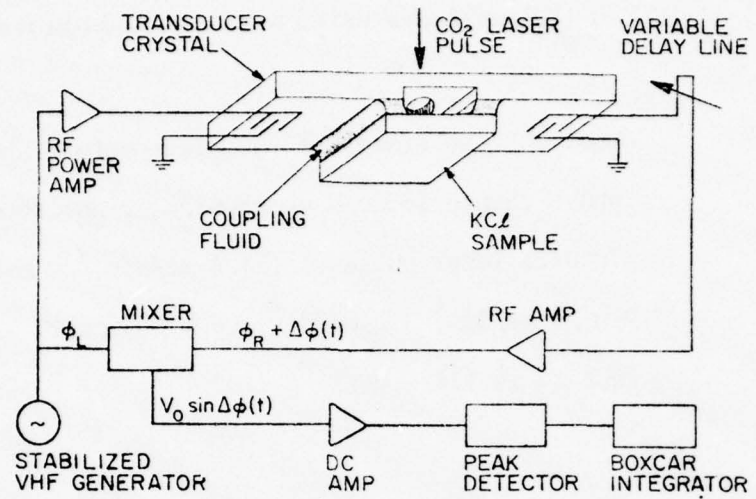


FIGURE 1

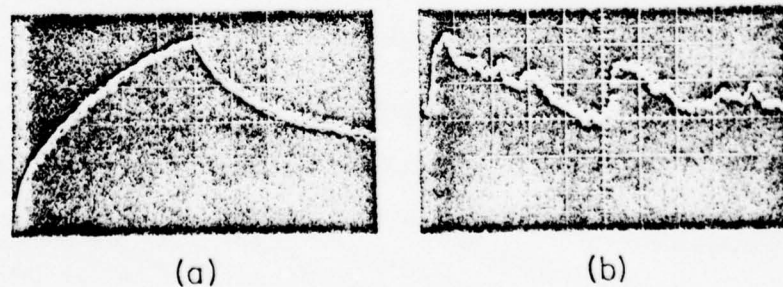


FIGURE 2

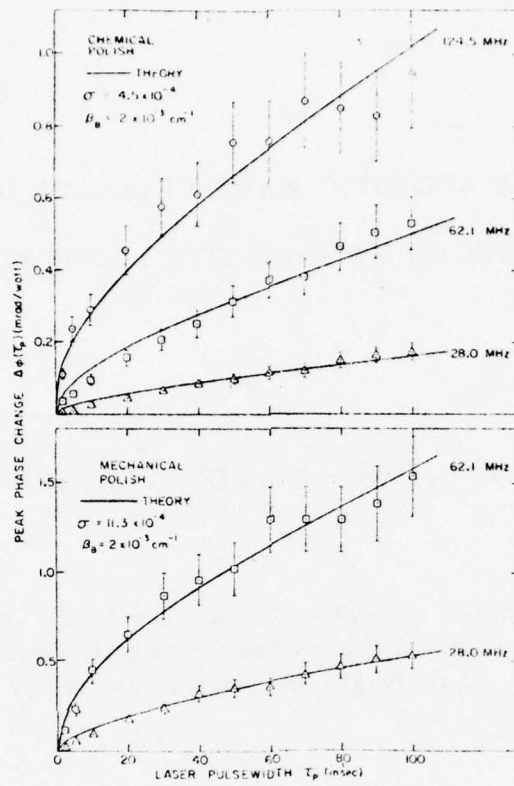


FIGURE 3

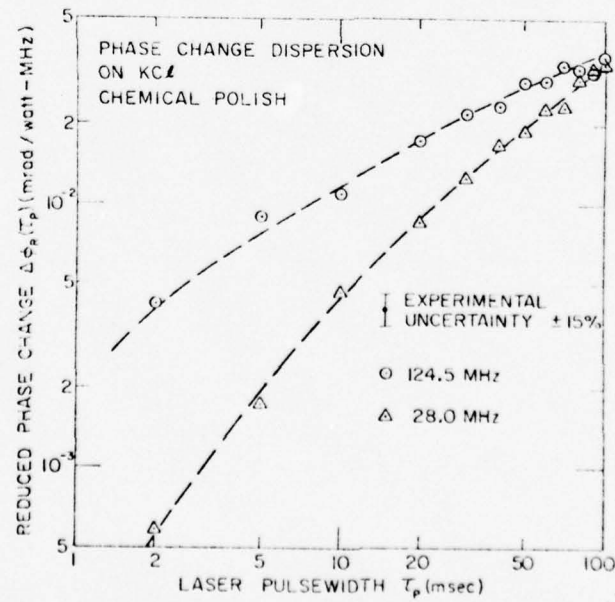


FIGURE 4

**SURFACE ACOUSTIC WAVE VELOCITY DISPERSION  
INDUCED BY RADIATIVE ABSORPTION\***

**J. H. Parks<sup>†</sup> and D. A. Rockwell<sup>‡</sup>**

**Departments of Physics and Electrical Engineering  
University of Southern California  
Los Angeles, California 90007**

## ABSTRACT

An analysis of the dispersive propagation of surface acoustic waves through a time dependent thermal gradient induced by radiative absorption is presented. The dispersive phase change of the acoustic wave is shown to depend on the details of the surface absorptive properties of the material. In particular, measurement of such induced phase changes can determine the parameters which characterize the surface depth dependence of the radiative absorption coefficient. This analysis is applied to two cases: (i) a strongly absorbing material and (ii) a highly transparent bulk material with an absorbing surface layer. The relative sensitivity to bulk and total surface absorption is discussed, as well as the radiative pulse conditions for which the absorption coefficient depth profile can be determined. This technique is applied to published results for 10.6  $\mu\text{m}$  radiative absorption on KCl surfaces for which the total surface layer absorption and the bulk absorption coefficient are individually measured. Additional applications to related surface measurements are discussed.

PACS Numbers: 78.50. - w, 81.80. +x, 68.90. +y

## I. INTRODUCTION

The application of surface acoustic wave techniques to detect and measure surface radiative absorption has been described in several previous publications. The emphasis in this earlier work centered on developing sensitive techniques to measure radiatively induced acoustic phase changes<sup>1,2,3</sup> on arbitrary materials, and deriving a detailed theoretical description of the thermal-surface wave interaction<sup>4</sup>. Although the observation and utility of induced dispersive propagation was discussed in Refs. 3 and 4, the primary concern was to develop a quantitative description of the simplest interaction, which occurs when the temperature is uniform over the depth profile of the surface wave. In this paper we present an analysis of dispersive surface wave propagation arising from the time dependent thermal gradient induced by radiative absorption.

The use of surface acoustic wave velocity dispersion to probe material surface properties has received considerable attention, and a review of these applications is available in Ref. 5. In general, the physical basis of dispersion arises from a perturbation of the elastic coefficients which exhibits an appreciable gradient within the surface wave penetration depth. The energy of a surface acoustic wave is largely confined to within a wavelength of the surface, so that probing the material surface with several different acoustic frequencies provides information about the depth variation of the perturbation. In most cases which have been studied the perturbation was static, and an accurate determination of the gradient relied on the use of many different

frequencies. This can be impractical when it is desired to study the surface of an arbitrary material on which surface wave excitation introduces additional experimental limitations such as restricted frequency range or surface contamination. In contrast, the thermal gradient resulting from radiative absorption evolves in time through heat diffusion. In this case, measurement of the time dependence of dispersive effects provides an experimental degree of freedom which eliminates the need for many frequencies and greatly simplifies data taking. Since the process of heat diffusion near the surface can be described reliably, the measurement and analysis of dispersive surface wave propagation can be applied to unravel the depth variation of the radiative surface properties of materials.

This paper will develop the analysis necessary for the application of these techniques. In Sec. II, the acoustic phase change is derived by relating the surface wave velocity dispersion to the temperature distribution arising from radiative absorption. Section III treats two limiting examples: (A) a strongly absorbing material and (B) a highly transparent material with an absorbing surface layer. The theory for example (B) is applied in detail to the problem of measuring weak surface absorption on KCl samples. Finally, Sec. IV discusses applications to several related problems.

## II. DISPERSIVE PHASE CHANGE

It was shown in Ref. 4 that perturbed surface wave propagation in a region heated by radiative absorption could be accurately described by the thermally induced time dependence of the acoustic phase given by

$$\phi(t) = \frac{2\pi\nu}{v_{so}} \int_{\text{path}} \left[ 1 - \frac{\Delta v_s(x, t)}{v_{so}} \right] dx \quad (1)$$

where  $\nu$  is the frequency,  $v_{so}$  is the unperturbed surface wave velocity, and  $\Delta v_s(x, t)$  is the change in the surface wave velocity due to the thermal variation of the elastic coefficients. The integral is taken over the total acoustic path length. The general experimental configuration is shown in Fig. 1. Laser radiation is incident on the surface midway along the acoustic path of length  $2L$ . The laser beam direction is normal to the surface, along the  $z$ -axis. The temperature dependence of the elastic coefficients is small enough ( $\sim 10^{-4}/^{\circ}\text{K}$ ) that it is appropriate to linearize the dependence of the acoustic wave vector  $K = 2\pi\nu/v_s$ , and subsequently the surface wave velocity, on the induced temperature change  $\Delta T(\vec{r}, t)$ .

In general, there is a contribution to  $\phi(t)$  which results from the change in total acoustic path length due to thermal expansion. In the case under consideration, absorbed laser radiation will heat a local region, but the surrounding cooler part of the crystal will constrain the thermal expansion, thereby inducing internal stresses. The constrained

thermal expansion is treated by replacing the mathematical increment  $dx$  by a physical distance in the crystal given by  $dx[1 + (\partial u / \partial x)]$ . The thermoelastic strain  $(\partial u / \partial x)$  is a measure of the change in the distance  $u$  between surface elements due to the nonuniform thermal stresses, and can be calculated<sup>6</sup> under the assumption of plane stress. It was pointed out previously<sup>4</sup> that the constrained thermal expansion present within a heated region having dimensions much less than the propagation path generally results in a contribution to the change in  $\phi(t)$  of less than a few percent. This path length expansion will be omitted in this paper. In addition, for the thermal perturbations under consideration, we assume the resulting thermoelastic stress has negligible effect on the wave velocity.

Under these conditions, the transient phase change induced by radiative absorption becomes

$$\Delta\phi(t) = -\frac{4\pi\nu}{v_{so}} f_B \int_0^L \left[ \frac{\Delta v_s(x, t)}{v_{so}} \right]_{\lambda_s} dx , \quad (2)$$

assuming an axially symmetric temperature distribution. The subscript  $\lambda_s$  indicates that, in general, the integrand depends on the acoustic wavelength. The line integral is taken through the center of the heated region. The factor  $f_B$  accounts for the incomplete overlap of the acoustic beamwidth and the temperature profile. It should be pointed out that since the depth or  $z$  dependence is of central importance, we consider the case in which  $\partial\Delta T / \partial x \ll \Delta T / \lambda_s$ , because surface wave reflections from the perturbed

region are negligible under the experimental conditions. In the derivation of Eq. (2), it is assumed that the time dependence of the perturbation is slow compared to an acoustic wave period. Equation (2) was derived<sup>4</sup> for an isotropic material, but we assume that it is equally valid for propagation in an arbitrary, anisotropic material along some specified crystal direction. The general problem is then reduced to developing a way to calculate  $\Delta v_s(x, t)$  associated with that direction.

The surface wave penetration depth normal to the surface is approximately  $\lambda_s$ , the acoustic wavelength. When the temperature distribution  $\Delta T(\vec{r}, t)$  is essentially uniform over this penetration depth, i.e.,  $\partial \Delta T / \partial z \ll \Delta T / \lambda_s$ , the velocity variation can be approximated by  $\Delta v_s \approx v_{so} \alpha_v \Delta T(x, t)$ . The velocity temperature coefficient  $\alpha_v$  has been experimentally determined for a few common surface wave materials including crystal quartz and lithium niobate. Experimental measurements of  $\Delta \phi$  for these materials were compared<sup>4</sup> with Eq. (2) using no adjustable parameters, and the quantitative agreement was within 5% where the theory was applicable. In those experiments, the radiative pulse widths were long enough for heat diffusion to produce a uniform temperature within the surface wave penetration depth. In this way, the need to account for propagation in the presence of an axial temperature gradient was avoided, and the resulting analysis provided a clear picture of the fundamental surface wave-thermal interaction leading to the induced

phase changes.

In general, depending on the surface wave frequency and the extent of thermal diffusion, the temperature is nonuniform over the surface wave penetration depth as indicated in Fig. 1. In the presence of such a spatial inhomogeneity, surface wave propagation becomes dispersive. The time dependent dispersive velocity change  $\Delta v_s(x, t)$  results from a thermal perturbation of the density and the elastic coefficients. In order to calculate  $\Delta\phi$  it will be necessary first to relate the temperature change to the radiative absorption parameters of the solid surface, and then to find  $\Delta v_s$  from a suitable dispersion theory.

#### A. Temperature Change Induced by Radiative Absorption

Radiative absorption of a monochromatic wave in a dielectric medium can be described by an absorption coefficient  $\beta \text{ cm}^{-1}$ , representing the fractional intensity absorbed per unit length, defined by

$$\vec{I}(r, z, t) = \hat{z} I_0(r, t) e^{- \int_0^z \beta(z') dz'} \quad (3)$$

where  $I(r, z, t)$  is the laser intensity propagating in the  $z$  direction at a depth  $z$  inside the surface of the material,  $I_0(r, t)$  is the intensity at the surface, and  $\hat{z}$  is a unit vector along the  $z$ -axis. The possibility of  $z$  dependence of the absorption coefficient is shown explicitly. Assuming a square temporal pulse of width  $\tau_p$  and a gaussian radial profile of halfwidth  $\alpha$  (HWHM), we have

$$I_o(r, t) = \frac{P \ln 2}{\pi \alpha^2} e^{-(r/\alpha)^2 \ln 2} \quad 0 < t < \tau_p \quad (4)$$

$$= 0 \quad t > \tau_p$$

where  $P$  is the total integrated power inside the material and will be related to experimentally determined quantities below.

The temperature change  $\Delta T(\vec{r}, t)$  resulting from the absorption is found from the heat equation

$$\rho C_p \frac{\partial \Delta T}{\partial t} - \kappa \nabla^2(\Delta T) = \dot{Q} \quad (5)$$

where  $\dot{Q} = -\nabla \cdot \vec{I}$  is the power absorbed per unit volume,  $\rho$  is the density,  $C_p$  is the heat capacity, and  $\kappa$  is the thermal conductivity of the material under study. During the radiative pulse  $0 < t < \tau_p$ , the laser heating source is given by

$$\dot{Q} = \beta(z) \left\{ \frac{P \ln 2}{\pi \alpha^2} e^{-(r/\alpha)^2 \ln 2} \right\} \cdot e^{-\int_0^z \beta(z') dz'} \quad (6)$$

For materials and pulsed widths considered in the present work, temperature gradients in the  $z$  direction are much greater than the radial gradients, with the result that radial heat diffusion is insignificant. (Solutions to the three dimensional heat equation based on the work of Olcer<sup>7</sup> are consistent with this approximation.) Consequently, the temperature change retains the gaussian radial dependence of the laser profile and Eq. (5) is reduced to a one dimensional problem by taking

$$\Delta T(\vec{r}, t) = e^{-(r/\alpha)^2 \ln 2} T(z, t) \quad (7a)$$

for which

$$\frac{\partial T}{\partial t} - D \frac{\partial^2 T}{\partial z^2} = - \frac{1}{\rho C_p} \frac{P \ln 2}{\pi \alpha^2} \cdot F(z) \quad (7b)$$

where  $D = \kappa/C_p \rho$  is the thermal diffusivity and

$$F(z) = S(z) \exp \left\{ - \int_0^z S(z') dz' \right\}. \quad (7c)$$

A solution is obtained for an isolated, infinite slab of thickness  $b$  with the initial condition  $T(z) = 0$ . Heat losses at the surfaces are neglected, yielding the boundary conditions  $\partial T/\partial z = 0$  at  $z = 0, b$ . The formal solution to Eq. (7) is written in the form of a Fourier series

$$T(z, t) = T_0(t) + \sum_{n=1}^{\infty} T_n(t) \cos K_n z \quad (8a)$$

$$F(z) = F_0 + \sum_{n=1}^{\infty} F_n \cos K_n z \quad (8b)$$

where  $K_n = n\pi/b$ . The equations for the Fourier coefficients are

$$T_n(t) = \frac{1}{\kappa} \frac{P \ln 2}{\pi \alpha^2} \frac{F_n}{K_n^2} \left( 1 - e^{-K_n^2 D t} \right) \text{ for } n > 1 \quad (9a)$$

and

$$T_0(t) = \frac{1}{\kappa} \frac{P \ln 2}{\pi \alpha^2} F_0 D t. \quad (9b)$$

The Fourier coefficient  $F_n$  of the heating function  $F(z)$  depends on the model used to represent the absorptive properties of the material.

Several examples of current interest will be presented in Section III.

### B. Dispersive Velocity Change

The velocity change will now be related to the temperature increase  $\Delta T(\vec{r}, t)$ . The starting point for a dispersion theory must consider the spatial scale of the material inhomogeneity. For example, if the inhomogeneity is concentrated within a depth much less than an acoustic wavelength, the boundary perturbation can be expressed concisely by an acoustic layer wave model<sup>8</sup>. However, in our case this situation will only be approached for the shortest times and lowest frequencies. For this reason, we choose to represent the inhomogeneity as a volume perturbation in the form of a gradual spatial variation of the elastic properties induced by a temperature change for which

$\frac{\partial \Delta T}{\partial z} \lesssim \Delta T/\lambda_s$ . Auld has derived<sup>9</sup> an expression relating the dispersive velocity change  $\Delta v_s = (v_s - v_{s0})$  to a volume perturbation

$$\frac{\Delta v_s}{v_{s0}} \approx \frac{v_{s0}}{4P_s} \int_0^\infty \left\{ -\Delta \rho \omega^2 U^* \cdot U + \nabla_s U^* : \Delta C : \nabla_s U \right\} dz \quad (10)$$

where  $\omega$  is the angular frequency,  $U$  is the unperturbed displacement vector, and  $\nabla_s U$  is the strain field.  $P_s$  is the unperturbed acoustic power flux in the  $\hat{x}$  direction given by  $P_s = -1/2 \int_0^\infty \text{Re}[\dot{U}^* \cdot T \cdot \hat{x}] dz$ , where  $T$  is the stress tensor. The elements of the perturbed

compliance tensor are

$$\Delta C_{ijkl} = C_{ijkl}^0 \epsilon \Delta T(\vec{r}, t) \quad (11a)$$

and the density perturbation is

$$\Delta \rho = \rho_0 \epsilon \rho \Delta T(\vec{r}, t). \quad (11b)$$

Here  $C_{ijkl}^0$  and  $\rho_0$  are the unperturbed values, and it is assumed  $\epsilon, \epsilon_\rho \ll 1$ . In general, the magnitude of  $\epsilon$  will be different for each elastic coefficient, but for simplicity the identifying subscripts are not shown.

In particular we are interested in the study of crystals exhibiting cubic symmetry such as the alkali-halides. The unperturbed displacement vector for a wave travelling along the (100) direction of a non-piezoelectric cubic is expressed in the form<sup>10</sup>

$$U = \begin{bmatrix} u_1(z) \exp i(\omega t - Kx) \\ 0 \\ -iu_3(z) \exp i(\omega t - Kx) \end{bmatrix} \quad (12)$$

where

$$u_1(z) = A_1 e^{-\alpha_1 Kz} + A_2 e^{-\alpha_2 Kz} \quad (13a)$$

$$u_3(z) = B_1 e^{-\alpha_1 Kz} + B_2 e^{-\alpha_2 Kz} \quad (13b)$$

and  $K = 2\pi/\lambda_s = \omega/v_{so}$ . The expressions defining the decay constants

$\alpha_i$  and the amplitudes  $A_i$  and  $B_i$  are shown in the Appendix. Application of the Cauchy conditions readily extends the present treatment to propagation on an isotropic elastic solid. However, to apply this analysis to an arbitrary propagation direction on an anisotropic solid of less symmetry would require numerical composite solutions<sup>11</sup> for the displacement vector.

Using Eqs. (7a) and (8a) to express  $\Delta T(\vec{r}, t)$ , the following form for the velocity change is derived

$$\left[ \frac{\Delta v_s(x, t)}{v_{so}} \right]_{\lambda_s} = \frac{\omega}{4P_s} \sum_{n=0}^{\infty} T_n(t) \left\{ \frac{h_1}{(2\alpha_1)^2 + (K_n/K)^2} + \frac{h_2}{(2\alpha_2)^2 + (K_n/K)^2} \right. \\ \left. + \frac{h_{12}}{(\alpha_1 + \alpha_2)^2 + (K_n/K)^2} \right\} \cdot e^{-(x/\alpha)^2 \ln 2} \quad (14)$$

where  $h_1$ ,  $h_2$ , and  $h_{12}$ , defined in the Appendix, are constants independent of  $K$  involving the unperturbed material constants, the perturbations  $\epsilon$ ,  $\epsilon_\rho$ , and parameters describing the displacement amplitudes. The factor  $\omega/4P_s$  (see Appendix) is also independent of  $K$  so that all the dispersive behavior is contained in the lorentzian terms within the brackets. However, the dispersive nature of  $\Delta v_s/v_{so}$  will be significant only if there are terms for which the Fourier wave vector is comparable to the surface wave decay constant,  $K_n \approx \alpha_i K$ , and for which

the magnitude of  $T_n$  is appreciable. In other words, the spatial distribution of the temperature relative to the wave penetration depth determines the extent of dispersive propagation. Dispersion measurements provide the important experimental link to the radiative absorption parameters near the surface because each  $\lambda_s$  provides a different weighted sum of the  $T_n$ . Fitting the data for several frequencies increases the accuracy with which the  $T_n$  and the absorption parameters are determined.

Finally, we express the induced phase change using Eqs. (2) and (14)

$$\begin{aligned} \Delta\phi(t) \simeq & -\frac{\omega}{v_{so}} \frac{1}{w} \operatorname{erf}\left(\frac{w}{2a} \sqrt{\ln 2}\right) \frac{P}{K} \\ & \times \left(\frac{\omega}{4P_s}\right) \sum_{n=0}^{\infty} \frac{F_n}{K_n^2} \left(1 - e^{-K_n^2 Dt}\right) \left\{ \frac{h_1}{(2\alpha_1)^2 + (K_n/K)^2} \right. \\ & \left. + \frac{h_2}{(2\alpha_2)^2 + (K_n/K)^2} + \frac{h_{12}}{(\alpha_1 + \alpha_2)^2 + (K_n/K)^2} \right\} \end{aligned} \quad (15)$$

in which the gaussian y dependence of  $\Delta T(\vec{r}, t)$  has been used to calculate<sup>4</sup>

$$f_B = \frac{a}{w} \sqrt{\frac{\pi}{\ln 2}} \operatorname{erf}\left(\frac{w}{2a} \sqrt{\ln 2}\right) \quad (16)$$

assuming a uniform acoustic beam of width w. It is interesting to note that the only dependence of the phase change on the laser halfwidth  $a$  is through the error function and this dependence is exceptionally weak for  $w/a \gtrsim 3.5$ . This form for  $\Delta\phi$  is immediately

applicable to the general problem of measuring detailed surface absorptive properties by simply specifying  $F_n$ . This will be considered in the next section.

### III. DISPERSIVE PHASE CHANGE MEASUREMENTS OF $\beta(z)$

In general, the absorptive properties of a solid within a depth of several microns from the surface may differ from the relatively well defined properties of the bulk material. This surface absorption depends on surface preparation, including mechanical polishing and chemical etching procedures, immediate environmental impurity adsorption, and perhaps on the effects of surface dislocations induced during sample preparation. The resulting effect of these surface perturbations can be described by taking the radiative absorption coefficient to be a function of depth below the surface  $\beta(z)$ . A simple absorption model will be used to represent the variation of the absorption coefficient: The absorbing surface region has a constant coefficient  $\beta = \beta_S \text{ cm}^{-1}$  which extends a characteristic distance  $d$  into the material at which depth a transition to the constant bulk value  $\beta = \beta_B \text{ cm}^{-1}$  occurs. This model adequately represents the material absorption properties in the region probed by the surface wave. Although the sharp transition from  $\beta_S$  to  $\beta_B$  is somewhat unphysical, thermal diffusion during a laser pulsewidth of  $\tau_p \gg 1 \mu\text{sec}$  causes the acoustic probe measurement to be relatively insensitive to the finer details of the model.

Using this model and Eqs. (7c) and (8b), it is a straightforward

calculation to show

$$F_n = \frac{2}{b} [ I_{Sn} + I_{Bn} ] \quad \text{for } n \geq 1 \quad (17a)$$

$$F_0 = \frac{1}{b} \left[ 1 - e^{-\beta_S d} e^{-\beta_B (b-d)} \right] \quad (17b)$$

where

$$I_{Sn} = \frac{\beta_S^2}{\beta_S^2 + K_n^2} \left[ 1 - e^{-\beta_S d} \left( \cos K_n d - \frac{K_n}{\beta_S} \sin K_n d \right) \right] \quad (18a)$$

$$I_{Bn} = \frac{\beta_B^2}{\beta_B^2 + K_n^2} e^{-\beta_S d} \left[ \left( \cos K_n d - \frac{K_n}{\beta_B} \sin K_n d \right) - (-1)^n e^{-\beta_B (b-d)} \right] \quad (18b)$$

Application to cases of interest are effectively characterized by the ratio of  $\sigma = \beta_S d$  to  $\beta_B b$  which determines the heating of the surface layer relative to the bulk material. Since the penetration depth of the surface wave is much less than the sample thickness, the resulting phase change is physically independent of the parameter  $b$ . However, we use the product  $\beta_B b$  to define a dimensionless quantity which can be compared with  $\sigma$ . We emphasize that the variation of  $\beta_B b$  should be considered as a change in the bulk coefficient  $\beta_B$  for constant  $b$ . In this section we consider the dispersive propagation resulting from two examples of radiative absorption: (a) a strongly absorbing material for

which  $\beta_B b \gg 1$ , and (b) a highly transparent material having an absorbing surface layer. In both cases experimental evidence of dispersion will be presented and in case (b) a detailed study of the sensitivity of  $\Delta\phi$  to absorptive parameters is discussed.

A. Strong Bulk Absorption:  $\beta_B b \gg 1$

Since the depth of the surface layers under consideration are on the order of  $d \approx 1 \mu\text{m}$ , the surface absorption  $\sigma$  is weak even if  $\beta_S$  is comparable to  $\beta_B$ . In the limit of strong bulk absorption we have  $\beta_B b \gg 1 \gg \sigma$  for which the significant terms of the Fourier sum can be approximated by

$$I_{Sn} \approx \frac{\beta_S^2}{\beta_S^2 + K_n^2} \sigma \quad (19)$$

$$I_{Bn} \approx \frac{\beta_B^2}{\beta_B^2 + K_n^2} (1 - \sigma)$$

Thus  $I_{Bn} \gg I_{Sn}$  for this case and the resulting dispersive phase change becomes

$$\Delta\phi(t) \simeq -\frac{\omega}{v_{so}} \frac{1}{w} \operatorname{erf} \left( \frac{w}{2a} \sqrt{t} \right) \frac{1}{\kappa} (1-R) P_i$$

$$\begin{aligned}
& \times \left( \frac{\omega}{4P_s} \right) \frac{1}{b} \left[ Dt \left\{ \frac{h_1}{(2\alpha_1)^2} + \frac{h_2}{(2\alpha_2)^2} + \frac{h_{12}}{(\alpha_1 + \alpha_2)^2} \right\} \right. \\
& + \sum_{n=1}^{\infty} \frac{2}{K_n^2} \frac{\beta_B^2}{\beta_B^2 + K_n^2} \left( 1 - e^{-K_n^2 Dt} \right) \left\{ \frac{h_1}{(2\alpha_1^2) + (K_n/K)^2} \right. \\
& \left. \left. + \frac{h_2}{(2\alpha_2)^2 + (K_n/K)^2} + \frac{h_{12}}{(\alpha_1 + \alpha_2)^2 + (K_n/K)^2} \right\} \right] \quad (20)
\end{aligned}$$

where the radiative power inside the material has been related to the Fresnel reflectivity  $R$  and the experimentally measured incident laser power  $P_i$  by  $P = (1-R) P_i$ .

The factors in the sum given by  $(\beta_B/K_n)^2 \{1 - \exp(-K_n^2 Dt)\} / (\beta_B^2 + K_n^2)$  determine a characteristic depth of the temperature distribution,  $z_T$ , which evolves in time through thermal diffusion. Dispersion will result when  $z_T$  is comparable to the acoustic penetration depth  $\sim (\alpha_i K_i)^{-1}$ . Since  $z_T$  is initially  $\approx (\beta_B)^{-1}$ , a necessary condition for dispersive effects is  $\alpha_i K_i \approx \beta_B$ . However, this is not a sufficient condition for all times, since  $z_T$  increases monotonically. Experimental evidence<sup>4</sup> of dispersion under these conditions is shown in Fig. 2 for surface wave propagation on Y-cut  $\alpha$ -quartz. Phase changes at acoustic frequencies of 125 MHz and 11 MHz were induced by the absorption of 10.6  $\mu\text{m}$  radiation, for which

$\beta_B \simeq 241 \text{ cm}^{-1}$  and  $\alpha_i K / \beta_B \simeq 2$  and .5 for these two frequencies respectively. Although Eq. (20) is strictly valid only for a cubic crystal, the observed dispersion on quartz shows qualitatively similar effects. Figure 2 shows the reduced phase change at the time  $\tau_p$  per watt of laser power  $P_i$ 

$$\Delta\phi_R = \Delta\phi / (\nu f_B P_i)$$
versus laser pulselength  $\tau_p$ . The reduced phase change is convenient in discussing dispersion since  $\Delta\phi_R$  eliminates the trivial linear frequency dependence in Eq. (15), and also the uninteresting effects arising from different acoustic profiles at each frequency. For laser pulselengths  $\tau_p \sim 100 \text{ msec}$  the temperature distribution has become essentially uniform over the 31 MHz wave penetration depth of  $\sim 100 \mu\text{m}$ . For these long times the curves of  $\Delta\phi_R$  vs.  $\tau_p$  for 124 MHz and 31 MHz converge indicating insignificant dispersion. However, for  $\tau_p = 2 \text{ msec}$ , the temperature distribution halfwidth is at a depth of only  $\sim 80 \mu\text{m}$  resulting in sizeable dispersion.

In this example, the dispersive phase change given by Eq. (20) provides a method for measuring an exceptionally large absorption coefficient without the necessity of using an impractically thin sample. For example, an absorption coefficient of even  $\beta_B \sim 10^4 \text{ cm}^{-1}$  could quite readily be determined with surface waves in the range of  $\nu \simeq 30 - 100 \text{ MHz}$ .

#### B. Surface Layer Absorption

Perhaps a more demanding application is the possibility of separating surface layer and bulk radiative absorption parameters in highly transparent materials. In particular, induced phase change

techniques offer an inherently sensitive determination of the surface absorption  $\sigma$  as will be shown in the following analysis of  $10.6 \mu\text{m}$  absorption on KCl surfaces. The bulk absorption coefficient at this radiative wavelength for high purity KCl can range<sup>12</sup> between  $\beta_B \approx 1 \times 10^{-3}$  to  $5 \times 10^{-5} \text{ cm}^{-1}$  depending on the growth procedure. The surface absorption can be as low as  $\sigma \approx 1 \times 10^{-4}$  for a chemically etched surface or as high as  $\sigma \approx 1 - 3 \times 10^{-3}$  for a mechanically polished surface. These ranges indicate the possibility of a sample having  $0.1 < \sigma/\beta_B b < 10$  and suggest that both terms in  $F_n$  given by Eq. (18) may be comparable. The phase change is then written

$$\begin{aligned}
 \Delta\phi(t) = & - \frac{\omega}{v_{so}} \frac{1}{w} \operatorname{erf} \left( \frac{w}{2a} \sqrt{\ln 2} \right) \frac{1}{\kappa} \left( \frac{1+R}{1-R} \right) P_t \\
 & \times \left( \frac{\omega}{4P_s} \right) \frac{1}{b} \left[ D_t \left\{ \frac{h_1}{(2\alpha_1)^2} + \frac{h_2}{(2\alpha_2)^2} + \frac{h_{12}}{(\alpha_1 + \alpha_2)^2} \right\} \left[ 1 - e^{-\beta_s d} e^{-\beta_B (b-d)} \right] \right. \\
 & + \sum_{n=1}^{\infty} \frac{2}{K_n^2} \cdot \left[ I_{Sn} + I_{Bn} \right] \left( 1 - e^{-\frac{K_n^2}{n} D_t} \right) \\
 & \left. \times \left\{ \frac{h_1}{(2\alpha_1)^2 + (K_n/K)^2} + \frac{h_2}{(2\alpha_2)^2 + (K_n/K)^2} + \frac{h_{12}}{(\alpha_1 + \alpha_2)^2 + (K_n/K)^2} \right\} \right]. \tag{21}
 \end{aligned}$$

In this case the laser power inside the material  $P = P_t(1+R)/(1-R)$  has been expressed in terms of  $P_t$  the power transmitted through the sample

which is a more appropriate experimental quantity for a weakly absorbing material. This power term approximately includes the effect of multiple reflections. Further details arising from the interference of multiply reflected optical field amplitudes are neglected here since the finesse of the sample, considered as an etalon, is extremely low for the reflectivity  $\sim 4\%$ .

The following analysis includes a parameter study to estimate the relative sensitivity of  $\Delta\phi$  to  $\sigma$ ,  $\beta_B$ , and the individual parameters  $\beta_S$  and  $d$  as a function of laser pulselength  $\tau_p$ . The logarithmic derivatives  $d(\ln \Delta\phi)/d(\ln \sigma)$  and  $d(\ln \Delta\phi)/d(\ln \beta_B)$  are useful for this purpose since they directly indicate the fractional change in  $\Delta\phi$  per fractional change in  $\sigma$  and  $\beta_B$ , respectively. In this analysis the material properties of KCl were used, for which the acoustic penetration depths (1/e point) are 32  $\mu\text{m}$  and 128  $\mu\text{m}$  at the frequencies 120 MHz and 30 MHz respectively. The phase change is evaluated at times  $t = \tau_p$  for which the dispersion theory is valid and the derivatives are numerically calculated.

In Fig. 3 the sensitivity to surface absorption  $\sigma$  is shown for three values of the ratio  $\sigma/\beta_B b = .1, 1, 10$ , keeping  $\beta_B = 10^{-3} \text{ cm}^{-1}$  and  $b = .1 \text{ cm}$  constant. As expected, the highest sensitivity is approached for shorter times and the largest ratio since the heating is more concentrated in the surface wave profile under these conditions. However, it is important to note that the sensitivity to  $\sigma$  is quite high even for  $\sigma/\beta_B b = 1$  at  $\tau_p = 10 \text{ msec}$ . At this pulselength, the temperature half-width is  $\sim 200 \mu\text{m}$  which is roughly a factor of 6 greater than the surface

wave penetration depth at 120 MHz. This suggests that the experimental conditions under which the integrated surface absorption can be readily measured are well within the technique's capability. The sensitivity to  $\sigma$  using a 120 MHz surface wave is shown in Fig. 3 to be only slightly greater than for a 30 MHz wave even though the penetration depth has changed by a factor of 4. This indicates that the overall sensitivity to  $\sigma$  is determined primarily by the surface temperature rather than by the temperature depth dependence.

The sensitivity to the bulk absorption coefficient  $\beta_B$  is shown in Fig. 4. The logarithmic derivative was calculated for three values of the ratio  $\sigma/\beta_B b = .1, 1, 10$ , keeping  $\sigma = 10^{-4}$  ( $\beta_S = 1 \text{ cm}^{-1}$ ,  $d = 10^{-4} \text{ cm}$ ) and  $b = .1 \text{ cm}$  constant. As the pulselwidth increases, heat diffusion mixes the bulk and surface thermal energy in the depth probed by the acoustic wave, resulting in an enhanced bulk sensitivity. It was previously indicated in Sec. A that for strongly absorbing materials, the ratio  $\sigma/\beta_B b$  is small and the phase change essentially measures only the bulk absorption. The approach to this limit is shown by the curve for  $\sigma/\beta_B b = .1$ . Conversely, when  $\sigma$  dominates, the sensitivity to bulk values becomes quite weak. It should be emphasized that these sensitivity curves in Figs. 3 and 4 will generally depend on the individual magnitudes of both  $\sigma$  and  $\beta_B b$  and not simply their ratio.

Figures 5 and 6 present phase change measurements obtained in recent studies<sup>13</sup> of surface absorption layers on chemically polished KCl. Figure 5 shows  $\Delta\phi$  versus laser pulselwidth for 124.5 MHz and 28.0 MHz

surface waves ( $\lambda_s = 14.1 \mu\text{m}$  and  $62.5 \mu\text{m}$ , respectively) with theoretical fits of Eq. (21) to the data for each frequency. These theoretical fits yield an average value for surface absorption of  $\sigma = (4.5 \pm .5) \times 10^{-4}$  and for bulk absorption  $\beta_B = (2 \pm .3) \times 10^{-3} \text{ cm}^{-1}$ . The ratio  $\sigma/\beta_B$  is 2 for these data indicates a relatively high sensitivity to  $\sigma$  for short times and high acoustic frequency, and low sensitivity to  $\beta_B$  except for longer  $\tau_p$ . Figure 6 shows the phase change dispersion in  $\Delta\phi_R$  versus laser pulse-width. The data for the two frequencies clearly diverge from each other for short times, well beyond experimental uncertainties of about  $\pm 15\%$ . This divergence is direct evidence that absorbing layers are present even after removing approximately  $10 \mu\text{m}$  of surface material by chemical polishing. The theory using the best fit parameters for  $\sigma$  and  $\beta_B$  represents an adequate description of the data except for the shorter times at 28.0 MHz. It is believed this short times discrepancy, which is emphasized by the log-log plot, arises from a breakdown of the volume perturbation calculation of  $(\Delta v/v_{so})$  when the characteristic depth  $z_T$  of the temperature distribution becomes comparable to the acoustic penetration depth which is  $\sim 2.2 \lambda_s$  for KCl. Temperature calculations indicate that the ratio of  $z_T$  to the acoustic penetration depth is only  $\sim 2$  at 20 msec and decreases to  $\sim .5$  at 2 msec. Because of the shorter penetration depth at 124.5 MHz (a factor of  $\sim 4$ ), the theory is adequate at that frequency even for the shortest times.

Finally, it is interesting to consider the conditions under which the phase change is sensitive to the individual parameters  $\beta_S$  and  $d$ .

Thermal diffusion is the primary limitation to such a separation of parameters since diffusion eliminates temperature differences over distances  $\sim d$  in a time  $\tau_d \sim d^2/D$ . In KCl,  $D = .048 \text{ cm}^2/\text{sec}$  which yields  $\tau_d = 200 \text{ nsec}$ , assuming a layer thickness of  $d = 10^{-4} \text{ cm}$ . Thus, it would be unreasonable to expect the induced phase change to be independently sensitive to  $d$  and  $\beta_S$  with laser pulsewidths  $\tau_p > 1 \mu\text{sec}$  for these conditions. The effect of thermal diffusion is shown in Fig. 7 which presents the temperature time evolution for  $\sigma_0 = 10^{-3}$ ,  $\beta_B = 10^{-5} \text{ cm}^{-1}$  and  $b = .1 \text{ cm}$ , a parameter set which assures a sensitivity only to surface absorption. The temperature is calculated for two cases: (i)  $\beta_S = 5 \text{ cm}^{-1}$ ,  $d = 2 \times 10^{-4} \text{ cm}$  and (ii)  $\beta_S = 2 \text{ cm}^{-1}$ ,  $d = 5 \times 10^{-4} \text{ cm}$ , and the percentage difference is shown as a function of laser pulsewidth. In Fig. 7a the peak surface temperatures are compared, and in Fig. 7b the depth of the temperature halfwidth for each case is shown. Clearly, for  $\tau_p > .1 \text{ msec}$  the temperature distribution depends only on  $\sigma_0$  which is the same for both cases. However, a Q-switched  $\text{CO}_2$  laser with  $\tau_p \simeq .5 \mu\text{sec}$ , or a TEA laser with  $\tau_p \simeq .1 \mu\text{sec}$  (total energy width), would certainly be useful to observe the individual dependence on the parameters  $\beta_S$  and  $d$  in KCl surface layers.

#### IV. CONCLUSION

The present theory describes the dispersive behavior of the thermal-acoustic interaction and properly accounts for this effect on the magnitude of the laser-induced phase change of a surface acoustic

wave. Although the analysis here has stressed cubic materials, it is quite straightforward to extend the present treatment to materials of arbitrary symmetry. In addition, the possibility of including a material inhomogeneity on a scale much less than the acoustic wavelength requires only minor revision. Experimental measurement of dispersive surface wave propagation offers the possibility of examining the detailed characteristics of radiative absorption at material surfaces. The facility of these techniques is enhanced by the time evolving thermal gradient which adds an experimental degree of freedom reducing the need for measurements at many different wavelengths. In addition, the experimental sensitivity inherent in phase measurements increases the utility of this technique.

We have considered two examples for analysis here: strong bulk absorption, and surface layer absorption in essentially transparent materials. The latter, a current problem in high power laser window technology, was examined more thoroughly to emphasize the sensitivity of phase change measurements to the intricate details of absorbing surface layers. Experimental results were presented indicating dispersive propagation of surface waves on KCl following absorption of 10.6  $\mu\text{m}$  radiation. Fitting the theory to the data provided a measurement of the integrated surface absorption  $\sigma$  as well as the bulk absorption coefficient  $\beta_B \text{ cm}^{-1}$ .

The application of this measurement technique to examine a wider range of surface phenomena may be considered. Certainly the layer

absorption model is particularly appropriate to describe absorption in a thin dielectric or metallic film deposited on an otherwise transparent substrate. This relates to the need to measure  $\sigma$  for highly reflecting films and protective film coatings associated with high power laser optics. The possibility of obtaining the spatial distribution of an absorption coefficient  $\beta(z)$  near a surface may be particularly interesting if the absorption is directly related to the diffusion of impurities into the surface. In this case a tuneable laser resonant at the impurity absorption would induce a thermal gradient sensitive to the particle diffusion properties. The availability of tuneable infrared lasers also suggests the possibility of tuning through restrahl resonances at the surface of a solid. Surface waves propagating on the solid surface would serve to detect these very high crystal absorptions without the need for fabricating thin samples. The theory developed in this paper establishes a starting point for the extension of these surface wave techniques to the study of a variety of surface processes with increased precision and sensitivity.

The authors wish to thank S. Allen and A. Timber of Hughes Research Laboratories for the KCl samples and their preparation. They also thank D. White and R. King of China Lake NWC for transducer fabrication, and D. Smith for his invaluable assistance in writing the computer programs.

## APPENDIX: DISPERSIVE PROPAGATION IN CUBIC MATERIALS

It is the purpose of this Appendix to derive an expression for the change in surface wave velocity induced by a subsurface thermal gradient in materials having cubic symmetry. The unperturbed solution<sup>10</sup> for the mechanical displacement vector will be presented. The velocity change can then be expressed in terms of this solution and the existing temperature distribution.

We begin with the wave equation for the displacement component of an elastic, anisotropic medium, in the absence of external body forces and piezoelectric effects:

$$\rho \frac{\partial^2 u_i}{\partial t^2} = c_{ijkl} \frac{\partial^2 u_k}{\partial x_j \partial x_l} + \frac{\partial u_k}{\partial x_l} \left[ \frac{\partial}{\partial x_j} c_{ijkl} \right] \quad (i, j, k, l = 1, 2, 3) \quad (A1)$$

The presence of the second term accounts for possible spatial variation in the elastic constants. In the present work, this variation is expressed in the form

$$c_{ijkl} = c_{ijkl} \left[ 1 + \epsilon_{ijkl} \Delta T(\vec{r}, t) \right] \quad (A2)$$

and the density variation

$$\rho = \rho_0 \left[ 1 + \epsilon_{\rho} \Delta T(\vec{r}, t) \right]. \quad (A3)$$

Here  $c_{ijkl}^0$  and  $\rho_0$  are the unperturbed values, and the dependence on the temperature increase  $\Delta T(\vec{r}, t)$  is weak since the coefficients  $\epsilon$ ,  $\epsilon_{ijkl} \lesssim 10^{-4}/^{\circ}\text{K}$  for materials under consideration. We consider surface wave propagation along a crystal symmetry direction taken as the x axis, and the normal to the surface is parallel to the z axis. We assume the x and z variation of  $\Delta T(\vec{r}, t)$  is slow enough that  $\partial c_{ijkl}^0 / \partial x \ll 2\pi c_{ijkl}^0 / \lambda_s$  and  $\partial c_{ijkl}^0 / \partial z \ll 2\pi c_{ijkl}^0 / \lambda_s$ , where  $\lambda_s$  is the acoustic wavelength. In this case the second term in Eq. (A1) may be neglected. This condition is readily satisfied in the presence of such small temperature coefficients. We have then, for slowly varying elastic properties

$$\rho \frac{\partial^2 u_i}{\partial t^2} = c_{ijkl} \frac{\partial^2 u_k}{\partial x_j \partial x_l} . \quad (\text{A4})$$

Solutions which represent a wave propagating parallel to the x-axis, decaying with increasing distance z from the surface  $z = 0$  and having no dependence on the y-coordinate are expressed in the form

$$u = \begin{bmatrix} u_1(z) \exp i(\omega t - Kx) \\ 0 \\ -i u_3(z) \exp i(\omega t - Kx) \end{bmatrix} \quad (\text{A5})$$

where

$$u_1(z) = A_1 e^{-\alpha_1 Kz} + A_2 e^{-\alpha_2 Kz} \quad (\text{A6})$$

$$u_3(z) = B_1 e^{-\alpha_1 Kz} + B_2 e^{-\alpha_2 Kz} \quad (A7)$$

for a surface wave of angular frequency  $\omega$ , unperturbed velocity  $v_{so}$ ,

and wave vector  $K = 2\pi/\lambda_s = \omega/v_{so}$ . The decay coefficients are determined by the pair of equations

$$\alpha_1^2 + \alpha_2^2 = \frac{1}{\gamma} \left[ (1 - \gamma R) + \gamma^2 (1 - R) - (\gamma + \gamma')^2 \right] \quad (A8)$$

$$(\alpha_1 \alpha_2)^2 = (1 - \gamma R) (1 - R) \quad (A9)$$

where  $\gamma = c_{44}^0/c_{11}^0$ ,  $\gamma' = c_{12}^0/c_{11}^0$  and  $R = \rho_0 v_{so}^2/c_{44}^0$  and the unperturbed elastic constants are expressed in reduced subscript notation  $c_{IJ}^0$ . The three amplitude ratios

$$b_i = \frac{B_i}{A_i} = \frac{\alpha_i (\gamma + \gamma')}{\gamma (1 - R) - \alpha_i^2} \quad (i = 1, 2) \quad (A10)$$

$$a_1 = \frac{A_2}{A_1} = - \frac{\alpha_1 + b_1}{\alpha_2 + b_2} \quad (A11)$$

specify the solution to within a constant determined by the total mechanical energy. Finally, the unperturbed acoustic power flux,  $P_s$ , is given by

$$\begin{aligned}
\frac{4P_s}{\omega} &= \frac{1}{\alpha_1} \left[ c_{11}^0 + c_{44}^0 b_1 (\alpha_1 + b_1) - c_{12}^0 \alpha_1 b_1 \right] \\
&+ \frac{a_1^2}{\alpha_2} \left[ c_{11}^0 + c_{44}^0 b_2 (\alpha_2 + b_2) - c_{12}^0 \alpha_2 b_2 \right] \\
&+ \frac{2a_1}{\alpha_1 + \alpha_2} \left[ 2c_{11}^0 + c_{44}^0 \left[ b_1 (\alpha_2 + b_2) + b_2 (\alpha_1 + b_1) \right] \right. \\
&\quad \left. - c_{12}^0 (\alpha_1 b_1 + \alpha_2 b_2) \right]. \tag{A12}
\end{aligned}$$

The dispersive velocity change induced by the presence of  $\Delta T(\vec{r}, t)$  is given by Eqs. (10) and (14) under the conditions discussed in Section II B. For the surface wave solution given above, the constants  $h_1$ ,  $h_2$  and  $h_{12}$  in Eq. (14) are given by

$$h_1 = 2\alpha_1 \left[ d_1 - v_{so}^2 \rho_0 \epsilon_p (1 + b_1^2) \right] \tag{A13}$$

$$h_2 = 2\alpha_2 a_1^2 \left[ d_2 - v_{so}^2 \rho_0 \epsilon_p (1 + b_2^2) \right] \tag{A14}$$

$$h_{12} = 2(\alpha_1 + \alpha_2) a_1 \left[ d_{12} - v_{so}^2 \rho_0 \epsilon_p (1 + b_1 b_2) \right] \tag{A15}$$

where

$$d_1 = c_{11}^0 \epsilon_{11} \left[ 1 + (\alpha_1 b_1)^2 \right] - 2c_{12}^0 \epsilon_{12} \alpha_1 b_1 + c_{44}^0 \epsilon_{44} (\alpha_1 + b_1)^2 \tag{A16}$$

$$d_2 = c_{11}^0 \epsilon_{11} \left[ 1 + (\alpha_2 b_2)^2 \right] - 2c_{12}^0 \epsilon_{12} \alpha_2 b_2 + c_{44}^0 \epsilon_{44} (\alpha_2 + b_2)^2 \quad (A17)$$

$$d_{12} = c_{11}^0 \epsilon_{11} \left[ 1 + \alpha_1 b_1 \alpha_2 b_2 \right] - c_{12}^0 \epsilon_{12} \left[ \alpha_1 b_1 + \alpha_2 b_2 \right] \\ + c_{44}^0 \epsilon_{44} (\alpha_1 + b_1)(\alpha_2 + b_2) . \quad (A18)$$

This completes the expressions needed to calculate the dispersive velocity change for wave propagation along a symmetry axis in cubic materials. Equations (A13) - (A18) and Eq. (21) have been applied to calculate phase changes induced by radiative absorption at KCl surfaces. The results of these calculations are shown in Figs. 5 and 6.

## REFERENCES

\* Research supported by the Advanced Research Projects Agency.

† Present address: Avco Everett Research Laboratory, Inc., Everett, Massachusetts 02149.

‡ Present address: Laser Division, Hughes Aircraft Company, Culver City, California 90230

1. J. H. Parks, D. A. Rockwell, T. S. Colbert, K. M. Lakin, and D. Mih, *Appl. Phys. Lett.* 25, 537 (1974).
2. D. A. Rockwell and J. H. Parks, *J. Appl. Phys.* 46, 5088 (1975).
3. D. A. Rockwell, T. S. Colbert, and J. H. Parks, in Proceedings of the International Conference on Optical Properties of Highly Transparent Solids, edited by S. S. Mitra and B. Bendow, (Plenum Press, New York, 1975), p. 493.
4. D. A. Rockwell and J. H. Parks, to be published in *J. Appl. Phys.*, manuscript no. 192R.
5. T. L. Szabo, *J. Appl. Phys.* 46, 1448 (1975).
6. B. A. Boley and J. H. Weiner, Theory of Thermal Stress (Wiley, New York, 1960).
7. N. Y. Olcer, *Int. J. Heat Mass Transfer* 8, 529 (1964).
8. B. A. Auld, Acoustic Fields and Waves in Solids (Wiley, New York, 1973), Vol. II, p. 272.
9. ibid., p. 294.
10. R. Stoneley, *Proc. Roy. Soc.* 232A, 447 (1955).
11. G. W. Farnell, in Physical Acoustics, Vol. 6, edited by W. P. Mason and R. N. Thurston (Academic, New York, 1970).
12. T. F. Deutsch, *Appl. Phys. Lett.* 25, 109 (1974).
13. D. A. Rockwell and J. H. Parks, submitted to *Appl. Phys. Lett.*, manuscript no. 1080L.

### FIGURE CAPTIONS

**Fig. 1** General experimental configuration for the study of radiatively induced, acoustic surface wave velocity dispersion. Incident laser radiation is absorbed in the shaded region which results in a temperature change having a depth distribution indicated by  $\Delta T(z, t)$ . This temperature distribution is probed by an acoustic surface wave of wave vector  $K_s$ , whose energy distribution is shown having a penetration depth comparable to the acoustic wave length  $\lambda_s$ . Coordinate axes shown are not intended to coincide with the crystal axes of the sample.

**Fig. 2** Phase change dispersion on Y-cut quartz as a function of laser pulselength. The reduced phase change per watt of incident laser power,  $\Delta\phi_R = \Delta\phi / (\nu f B_i P_i)$ , is shown for acoustic frequencies of 31 MHz and 124 MHz. Dashed curves are shown as guides to the eye.

**Fig. 3** The relative sensitivity of the induced phase change to the integrated surface absorption  $\sigma$  is indicated by the logarithmic derivative  $d(\ln \Delta\phi)/d(\ln \sigma)$  as a function of laser pulselength. This is shown for three values of the parameter ratio  $\sigma/\beta_B b$ , keeping  $\beta_B = 10^{-3} \text{ cm}^{-1}$  and  $b = .1 \text{ cm}$  constant. Curves are shown for acoustic frequencies of 120 MHz and 30 MHz.

**Fig. 4** The relative sensitivity of the induced phase change to the bulk absorption coefficient  $\beta_B$  is indicated by the logarithmic derivative  $d(\ln \Delta\phi)/d(\ln \beta_B)$  as a function of laser pulselength. This is shown for three values of the parameter ratio  $\sigma/\beta_B b$ , keeping  $\sigma = 10^{-4}$  ( $\beta_S = 1 \text{ cm}^{-1}$ ,  $d = 10^{-4} \text{ cm}$ ) and

$b = .1$  cm constant. Curves are shown for acoustic frequencies of 120 MHz and 30 MHz.

**Fig. 5** Phase change data versus laser pulselength for a chemically polished KCl surface at acoustic wave frequencies of 124.5 MHz and 28.0 MHz. Bars indicate  $\pm 15\%$  experimental uncertainty. Solid curves are theoretical fits to the data for each frequency. The average value of  $\sigma$  and  $\beta_B$  obtained from the best fit are indicated.

**Fig. 6** Phase change dispersion versus laser pulselength is indicated by the increasing divergence of  $\Delta\phi_R$  as  $\tau_p$  decreases. These data were taken on a chemically polished KCl surface at acoustic wave frequencies of 124.5 MHz and 28.0 MHz; experimental uncertainty of  $\pm 15\%$  is indicated for each data point by the bar. Solid curves are theoretical fits to the data for both frequencies. The average value of  $\sigma$  and  $\beta_B$  obtained from the best fit are indicated.

**Fig. 7** Measurement sensitivity to individual values of absorption parameters  $\beta_S$  and  $d$  depends strongly on thermal diffusion. This is indicated in (a) by comparing the peak surface temperatures versus laser pulselength.  $T_2$  is calculated using  $\beta_S = 2 \text{ cm}^{-1}$ ,  $d = 5 \times 10^{-4} \text{ cm}$  and  $T_5$  using  $\beta_S = 5 \text{ cm}^{-1}$ ,  $d = 2 \times 10^{-4} \text{ cm}$ . In (b) the halfwidth of the temperature depth distribution versus laser pulselength is shown for these same parameter sets.

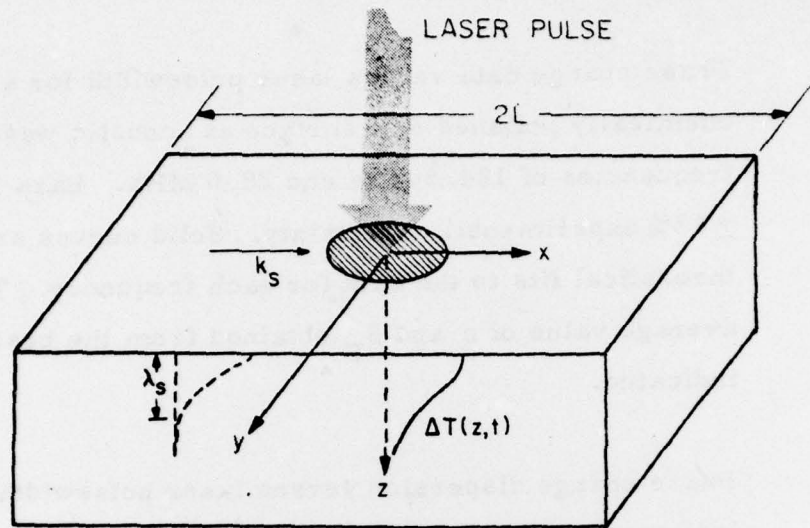


FIGURE 1

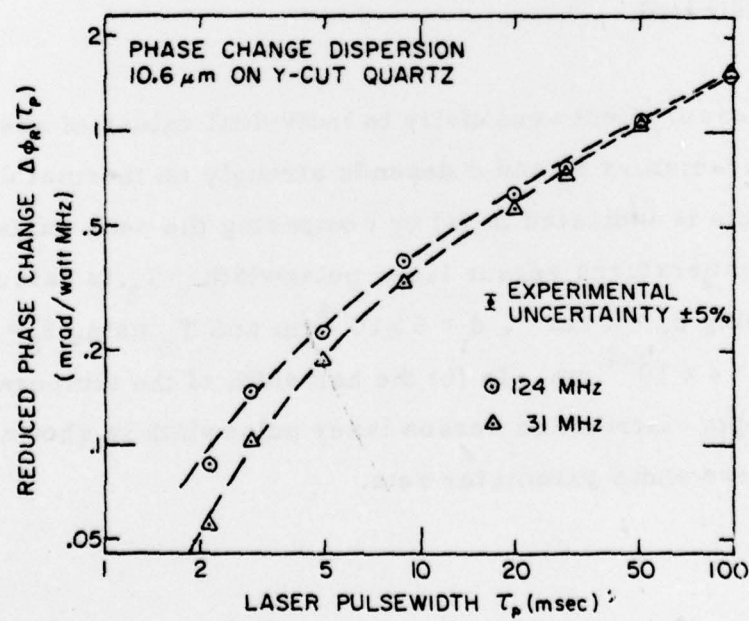


FIGURE 2

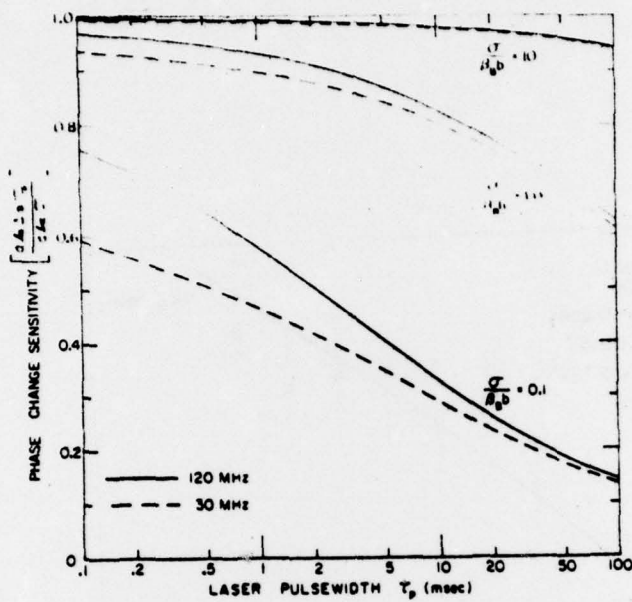


FIGURE 3

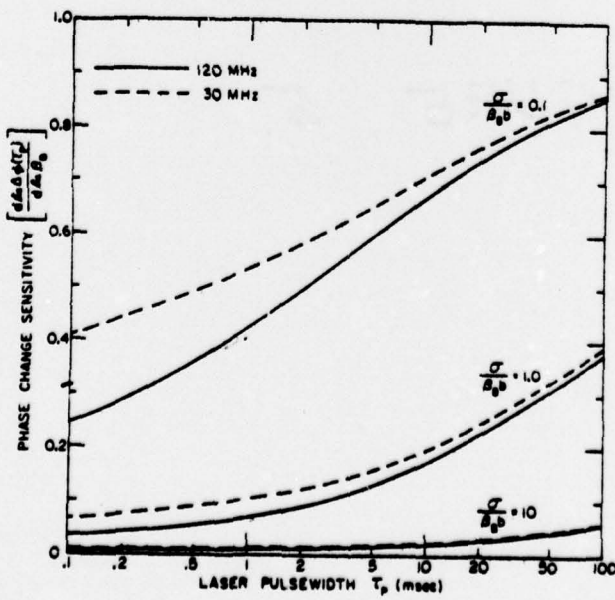


FIGURE 4 95

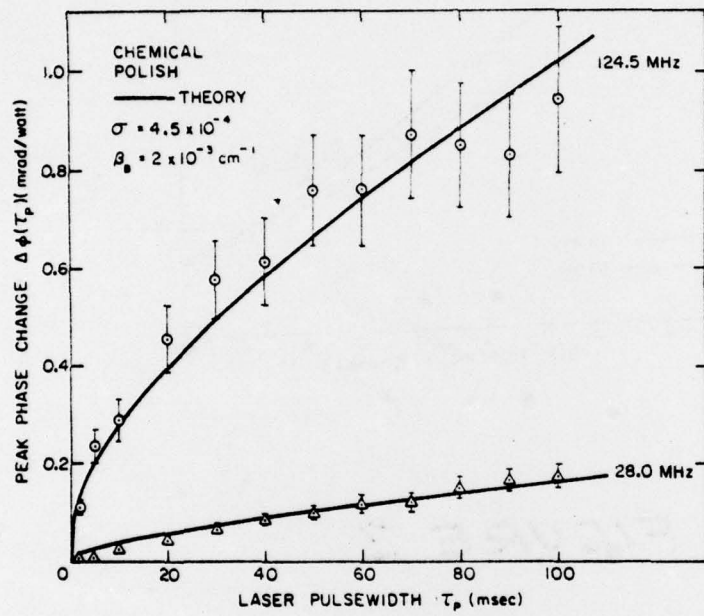


FIGURE 5

FIGURE 6

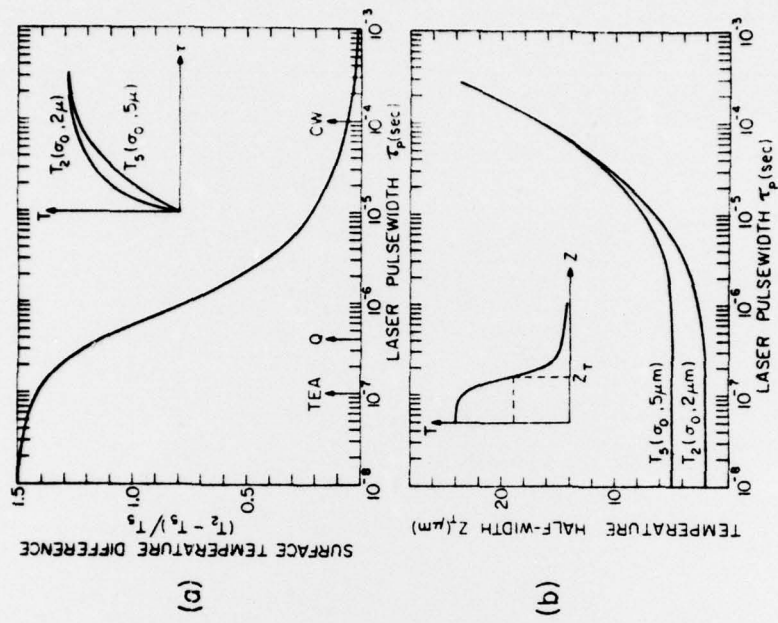
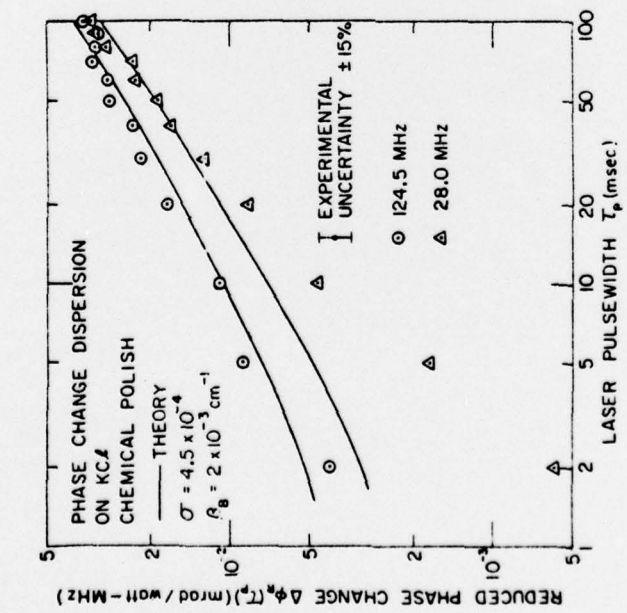


FIGURE 7

MISSION  
of  
*Rome Air Development Center*

RADC plans and conducts research, exploratory and advanced development programs in command, control, and communications (C<sup>3</sup>) activities, and in the C<sup>3</sup> areas of information sciences and intelligence. The principal technical mission areas are communications, electromagnetic guidance and control, surveillance of ground and aerospace objects, intelligence data collection and handling, information system technology, ionospheric propagation, solid state sciences, microwave physics and electronic reliability, maintainability and compatibility.

